# 21
# Ion Exchange

**Howard S. Sherry**
*University of New Mexico, Albuquerque, New Mexico, U.S.A.*

## I. INTRODUCTION

The most important technique used to modify zeolites is ion exchange. This chapter will review the ion-exchange properties of aluminosilicate zeolites with some emphasis on the problems and pitfalls encountered by this author. The techniques used to collect and analyze ion exchange data will be described. The data will be presented in the form of ion-exchange isotherms. These isotherms can be used to calculate thermodynamic quantities in the equilibrium case (1), in the design of experiments (2), and in commercial ion-exchange processes (2).

Zeolite structure will be discussed as it relates to the ion-exchange properties of the zeolites that will be used as examples. The dimensions of the channels and openings into cavities are of molecular and ionic size. Some quite spectacular molecular separations can be made by taking advantage of differences between molecular size and channel or window size. The openings into cavities and size of the channels can often be modified by ion exchange. Ion sieving, first reported by Barrer in 1956 (3), enables interesting and useful ion separations. The ability of zeolites to undergo ion exchange is one of their most important properties. It enables us to modify the electric field inside zeolite crystals, which in turn modifies sorptive and catalytic properties in a way that is more subtle than simple molecular sieving.

## II. EXPERIMENTAL TECHNIQUES

### A. Zeolite Preparation

Careful preparation and characterization of the zeolite being studied is extremely important if meaningful data are to be obtained. One of the most common problems in sample preparation is overwashing (5). It is important that the sample have a good cation balance. The atomic ratio of charge-balancing cations to aluminum atoms should be 1. In the case of a zeolite synthesized in the sodium form, that means that the atomic ratio Na/Al should be equal to 1. In our experience a ratio of $1.00 \pm 0.02$ is an acceptable result. It is extremely easy to reduce this ratio to less than 1 by extensive washing of the more aluminous zeolites such as NaA and NaX and even NaY. One can think of the zeolites as salts of weak acids. Therefore, if the sodium zeolite, NaZ, is placed in water, the zeolite hydrolyzes according to the reaction:

$$NaZ + 2HOH \rightleftharpoons H_3OZ + NaOH \tag{1}$$

Copyright © 2003 Marcel Dekker, Inc.

The pH of the water in which the zeolite is placed rises as proof that this reaction has taken place. Repeated contact with fresh water as might occur if a small quantity of the sodium form of the zeolite is extensively washed on a filter can lead to extensive $H_3O^+$ ion exchange. We have observed that as much as 15% of the $Na^+$ in NaA can be replaced by $H_3O^+$ by overwashing. We have controlled the $H_3O^+$ ion exchange of zeolites synthesized in the sodium form by careful washing until the Na/Al atomic ratio was $1.00 \pm 0.02$ (5). We have preconditioned zeolite samples not prepared by us by contacting the zeolite several times with 0.1 N NaCl (10% by weight slurry).

It has been shown (6) that when a zeolite is placed in water there is reaction at the surface of the crystals that causes a small amount of Si and Al to dissolve. This complicates ion exchange involving trace quantities of ions. However, under the ion-exchange conditions normally used for preparation of catalysts and sorbents, the effect is hidden by the analytical accuracy of the measurements and reversible equilibria are obtained.

A convenient way to store a batch of zeolite for ion-exchange studies is to store the carefully washed material in a chamber or vessel over a saturated aqueous solution of $NH_4Cl$ (7). This procedure maintains the zeolite with a constant water content because the water activity of a saturated $NH_4Cl$ solution does not change much with small changes in temperature.

Needless to say, the silica to alumina mole ratio (SAR) and X-ray crystal purity of the zeolite being studied has to be carefully determined. We have always used phase-pure, highly crystalline materials for our ion-exchange studies.

### B. Ion-Exchange Measurements and Presentation of the Data

Ion-exchange data are obtained by contacting a quantity of zeolite with a quantity of solution for a period of time at constant temperature, separating the two phases, and analyzing the solution and/or the zeolite to ascertain the composition of the exchanging ions. Usually, the solution is aqueous. The contact time is usually sufficient to attain equilibrium although that is not always necessary in the case of the design of commercial processes. The solution normality is almost always held constant to facilitate interpretation of the data.

As an example, consider the ion-exchange isotherm for the Li-Na-X system at 0.1 total normality of chloride solution and 25°C shown in Fig. 1 (5). The reaction is:

$$Li_s^+ + Na_z^+ \rightleftharpoons Li_z^+ + Na_s^+ \tag{2}$$

The subscripts s and z refer to the solution and zeolite phases. In Fig. 1 the abscissa is the equivalent fraction of ions in solution that are $Li^+$ and the ordinate is the equivalent fraction of ions in the zeolite that are $Li^+$.

$$S = \frac{\text{equivalents of } Li^+ \text{ in solution}}{\text{equivalents of } Li^+ + Na^+ \text{ in solution}} \tag{3}$$

$$Z = \frac{\text{equivalents of } Li^+ \text{ in zeolite}}{\text{equivalents of } Li^+ + Na^+ \text{ in zeolite}} \tag{4a}$$

The equivalent fraction of ions in the zeolite can also be expressed as

$$Z = \frac{\text{equivalents of } Li^+ \text{ in zeolite}}{g \text{ atoms of Al in the zeolite}} \tag{4b}$$

Copyright © 2003 Marcel Dekker, Inc.

because there is an equivalent of charge-balancing cation in the zeolite for each *g* atom of Al.

An example of di-univalent ion exchange is shown in Fig. 14 (6) in which we have plotted the data for the Ca-Na-A system at 0.1 total normality and 25°C. The reaction is:

$$Ca_s^{2+} + 2Na_z^{+} \rightleftharpoons Ca_z^{2+} + 2Na_s^{+} \tag{5}$$

Visual inspection of the ion-exchange isotherm allows us to make some conclusions as to the preference of the zeolite for the ingoing or outgoing cation. If we draw a line through the points (0,0) and (1,1) in Fig. 1 or Fig. 2 we obtain the unit selectivity line. If the isotherm is described by this line, then the zeolite has no preference for the ingoing ion over the outgoing ion. If the isotherm lies above the unit selectivity line, then the zeolite prefers the ingoing ion. In the parlance of ion exchange we say that the zeolite is selective for the ingoing ion. The isotherm for the Ag-Na-X system shown if Fig. 5 indicates that zeolite NaX is very selective for, or strongly prefers, $Ag^+$. By contrast, the isotherm in Fig. 1 indicates that zeolite X is very selective for $Na^+$ over $Li^+$ (5).

A similar graphical representation of ion-exchange isotherms was used by Professor R. M. Barrer and is still used by his students and their students. In their plots of the data the abscissa is Z and the ordinate is S. Isotherms are plotted using either scheme throughout the literature. Visual inspection of the isotherms allows the same conclusions to be reached in either case.

## III. ION EXCHANGE IN ZEOLITES X AND Y

### A. Uni-Univalent Ion Exchange

A very thorough study of ion-exchange equilibria in the synthetic zeolites X and Y was done by Sherry (5) and Barrer and Rees (8–10). The isotherms for $Li^+$, $K^+$, $Rb^+$, $Cs^+$, $Ag^+$, and $Tl^+$ ion exchange of NaX at 25°C and 0.1 total normality are shown in Figs. 1–6. The anion is $Cl^-$ for the alkali metal ions and $NO_3^-$ for the $Ag^+$ and $Tl^+$ systems. The Li-Na isotherm was discussed above. The K-Na isotherm winds around the

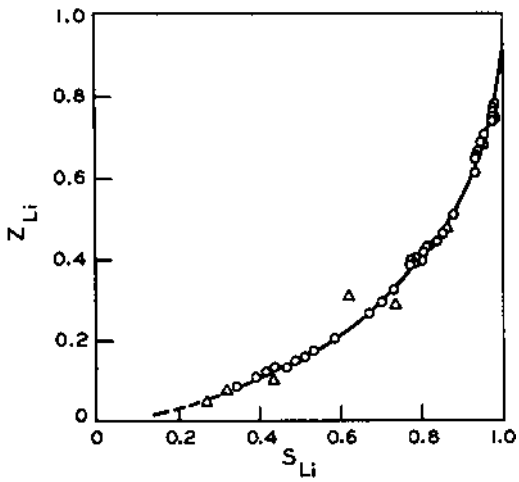


**Fig. 1** The ion-exchange isotherm for the Li-Na-X system at 0.1 total normality and 25°C. ○, $Li_s^+ + Na_z^+$; Δ, $Na_s^+ + Li_z^+$. (From Ref. 5.)

Copyright © 2003 Marcel Dekker, Inc.

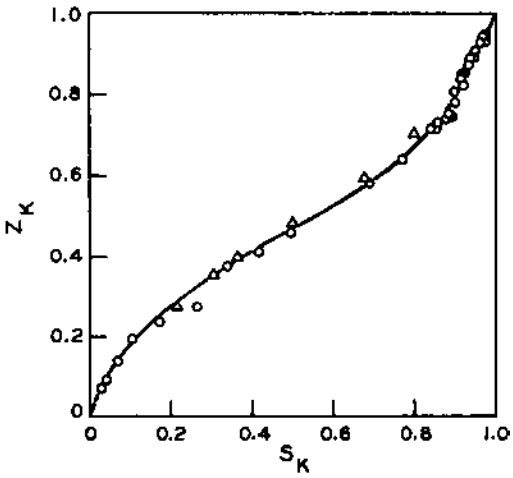


**Fig. 2** The ion-exchange isotherm for the K-Na-X system at 0.1 total normality and 25°C. ○, $K_s^+ + Na_z^+$; Δ, $Na_s^+ + K_z^+$. (From Ref. 5.)

unit selectivity line. At low $K^+$ loading, zeolite NaX shows a slight preference for $K^+$ and at higher loading this preference reverses.

The isotherms at 25°C for $Li^+$, $K^+$, $Rb^+$, $Cs^+$, $Ag^+$, and $Tl^+$ ion exchange of NaY taken from Sherry (5) are shown in Figs. 7–12. The Li-Na and K-Na isotherms resemble those for zeolite X. The Rb-Na and Cs-Na isotherms for zeolite Y are different from those for zeolite X in that they show a definite termination at about 68% exchange. The Tl-Na isotherm also shows a definite termination at 68% exchange in zeolite Y.

The differences in the uni-univalent ion exchange properties of zeolites X and Y can be understood in terms of their framework structure and the location of the cations that balance the negative charges on the aluminosilicate framework. The structure of the

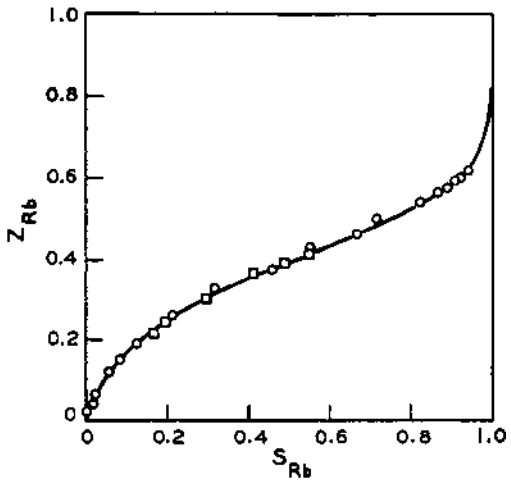


**Fig. 3** The ion-exchange isotherm for the Rb-Na-X system at 0.1 total normality and 25°C. ○, $Rb_s^+ + Na_z^+$; □, $Na_s^+ + Rb_z^+$. (From Ref. 5.)

Copyright © 2003 Marcel Dekker, Inc.

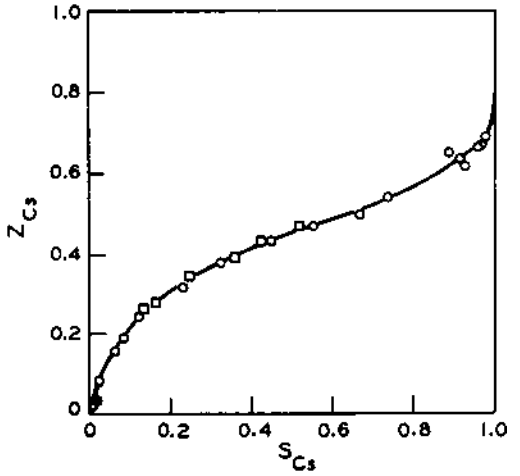


**Fig. 4** The ion-exchange isotherm for the Cs-Na-X system at 0.1 total normality and 25°C. ○, $Cs_s^+ + Na_z^+$. (From Ref. 5.)

aluminosilicate framework is the same for zeolites X and Y (11). Both are isostructural with the natural zeolite, faujasite (12). This framework structure is shown in Fig. 13. The faujasite structure can be formed by arranging sodalite cages in a tetrahedral array, as carbon atoms are connected in diamond. Pairs of sodalite cages are linked through rings of six shared oxygen atoms to form hexagonal prisms. The tetrahedral array of sodalite cages enfolds much larger cages, often called supercages. The entrances to the sodalite cages are small rings of six tetrahedra (rings of $AlO_2$ and $SiO_2$ groups, six-rings). The entrances to the supercages are large rings of 12 tetrahedra (12-rings).

An early X-ray powder diffraction study (13) of a hydrated NaX containing 80 Na atoms per unit cell showed that 16 Na atoms per unit cell were located in the hexagonal

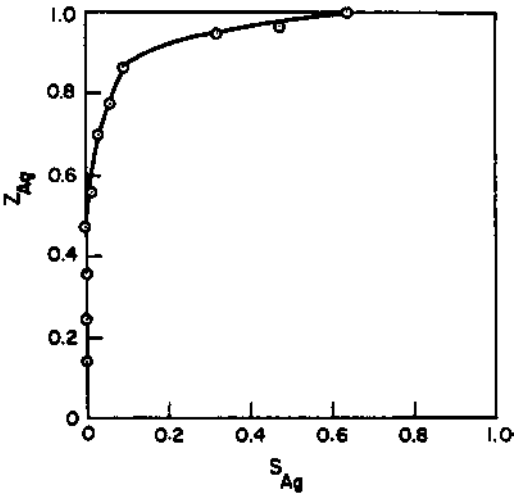


**Fig. 5** The ion exchange isotherm for the Ag-Na-X system at 0.1 total normality and 25°C. ○, $Ag_s^+ + Na_z^+$. (From Ref. 5.)

Copyright © 2003 Marcel Dekker, Inc.

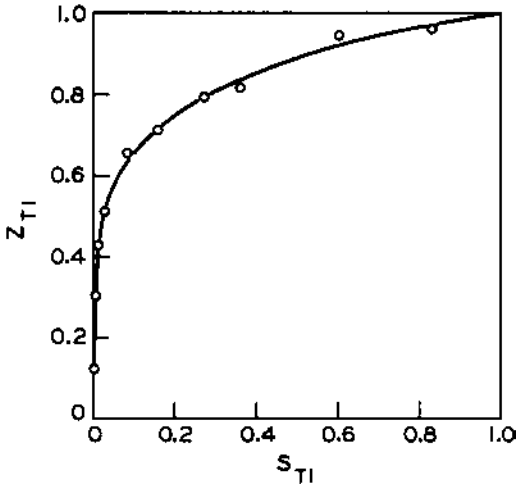


**Fig. 6** The ion-exchange isotherm for the Tl-Na-X system at 0.1 total normality and 25°C. ○, $Tl_s^+ + Na_z^+$ (From Ref. 5.)

prisms, one in each of the 16 hexagonal prisms per unit cell. Of the remaining cations, 32 were in the supercages located near the rings of 6 tetrahedra that are the connecting "windows" between the supercages and the sodalite cages. The remaining cations could not be located by X-ray powder diffraction and were believed to be mobile, hydrated ions in the supercages.

A study of a single crystal of NaX by D. H., Olson (14) found 4 Na atoms per unit cell in the hexagonal prisms, 8 in the sodalite cages, and 24 in the supercages near the center of the rings of 6 tetrahedra. Again, the remainder could not be located and were presumed to be mobile, hydrated cations in the supercages. The X-ray structure determination of hydrated faujasites (12) showed that there are 17 cations in the 8 sodalite cages that are in

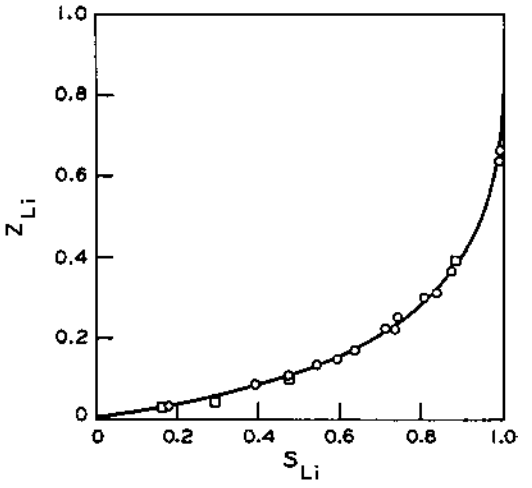


**Fig. 7** The ion-exchange isotherm for the Li-Na-Y system at 0.1 total normality and 25°C. ○, $Li_s^+ + Na_z^+$; □ $Na_s^+ + Li_s^+$. (From Ref. 5.)

Copyright © 2003 Marcel Dekker, Inc.

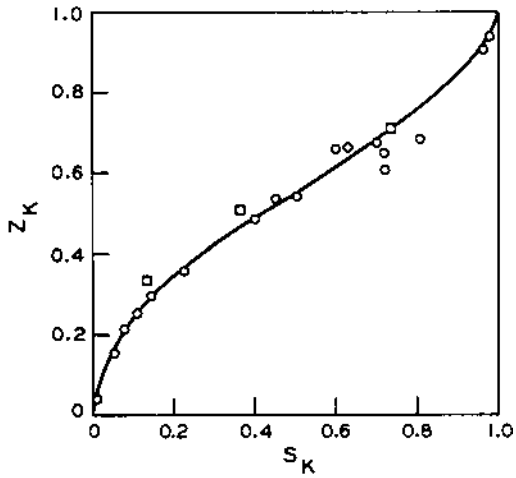


**Fig. 8** The ion –exchange isotherm for the K-Na-Y system at 0.1 total normality and 25°C: ○, $K_s^+ + Na_z^+$; □ $Na_s^+ + K_z^+$. (From Ref. 5.)

a unit cell. All of the structural studies agree that there are 16 or 17 cations in the network of sodalite cages and hexagonal prisms (network of small cages).

The structural factors that are important for understanding ion exchange are that the exchanging cations must diffuse through a series of rings of 12 tetrahedra (12-rings) with a free diameter of 8–9 Å (13) in order for ion exchange to occur in the supercages. They must diffuse from these large cages through a 6-ring with a free diameter of 2.5Å (13) in order for the ingoing ions to replace the $Na^+$ ions located in the network of small cages.

The Rb-Na-Y and Cs-Na-Y isotherms in Figs. 9 and 10 show that 32% of the $Na^+$ ions cannot be replaced. This particular NaY has a silica to alumina mole ratio (SAR) of 5.6. It contains 50 $Na^+$ per unit cell. Thus, the number of $Na^+$ per unit cell that cannot be

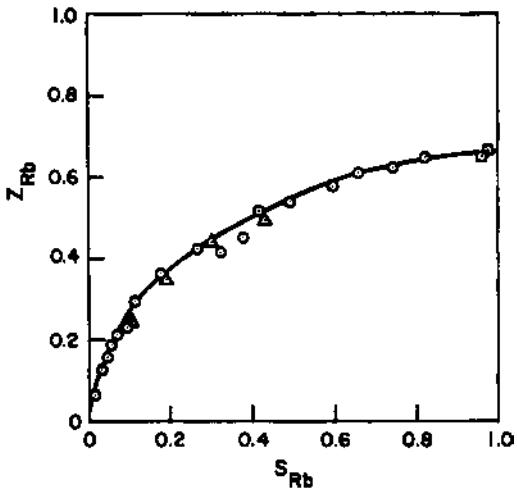


**Fig. 9** The ion-exchange isotherm for the Rb-Na-Y system at 0.1 total normality and 25°C. ○, $Rb_s^+ + Na_z^+$; Δ $Na_s^+ + Rb_z^+$. (From Ref. 5.)

Copyright © 2003 Marcel Dekker, Inc.

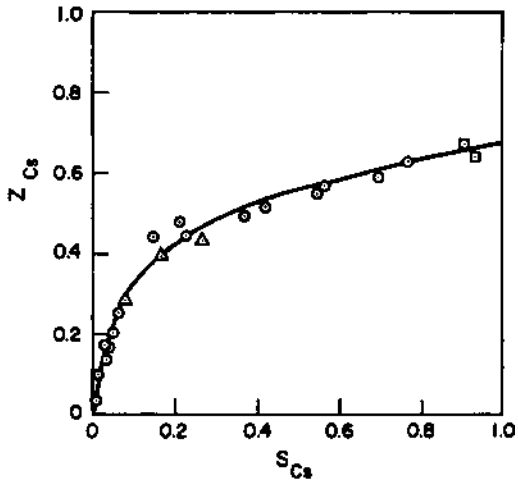


**Fig. 10** The ion-exchange isotherm for the Cs-Na-Y system at 0.1 total normality and 25°C. ○, $Cs_s^+ + Na_z^+$; Δ $Na_s^+ + Cs_z^+$. (From Ref. 5.)

replaced by $Rb^+$ and $Cs^+$ is 16, or 32% of the total. This result is not unexpected because the crystal radii of $Rb^+$ and $Cs^+$ are 1.48 and 1.69 Å (15), and they are too large to diffuse through the 6-rings that are the entrances to the sodalite cages and hexagonal prisms.

$Rb^+$ and $Cs^+$ exchange of NaX is less easy to understand because the point at which their isotherms terminate is not clear. This particular NaX has 85 $Na^+$ in a unit cell (2.56 SAR) and therefore 69 cations are in the large cages. Both Sherry (5) and Barrer et al. (10) showed that 32% of the cations, or 32 per unit cell could not be replaced by $Rb^+$ and $Cs^+$. In the latter study (10) it was suggested that at higher loadings these large cations crowd $Na^+$ into the small cages—a volume effect.

If we examine the ion-exchange isotherms in Figs. 1–12 at low loading of the incoming ion, the selectivity series that we obtain for alkali metal cations is Cs > Rb > K > Na  Li for

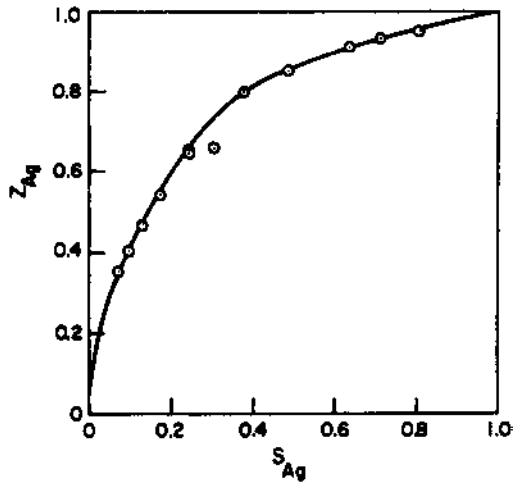


**Fig. 11** The ion-exchange isotherm for the Ag-Na-Y system at 0.1 total normality and 25°C. ○, $Ag_s^+ + Na_z^+$. (From Ref. 5.)

Copyright © 2003 Marcel Dekker, Inc.

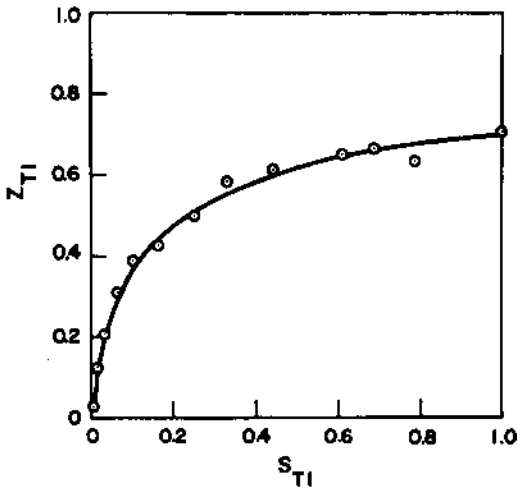


**Fig. 12** The ion-exchange isotherm for the Tl-Na-Y system at 0.1 total normality and 25°C. ○, $Tl_s^+ + Na_z^+$. (From Ref. 5.)

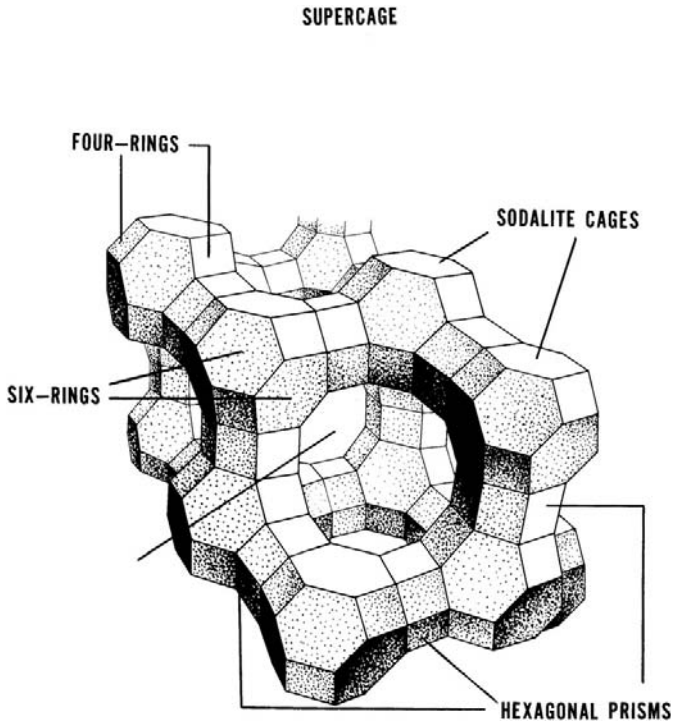


**Fig. 13** The framework structure of synthetic faujasite. (From Ref. 44.)

Copyright © 2003 Marcel Dekker, Inc.

zeolites X and Y. This is the selectivity series we would expect if the mobile, hydrated ions in the large cages are replaced. At 50–60% exchange the selectivity series that is observed for zeolites X and Y are Na > K > Rb ≫ Cs ≫ Li and Cs > Rb > K > Na ≫ Li. The selectivity series of zeolite X can best be accounted for by the exchange of ions located in the large cages but near to, and coordinated to, framework oxygen atoms of the 6-rings. Thus, except for $Li^+$ ions, the ion selectivity decreases with increasing ionic radius because bare, or partially bare, ions must interact with framework oxygen atoms. $Li^+$ is an exception because of its high hydration energy (15). In terms of this model, all of the ions in the large cages of zeolite Y are hydrated and not sited because the selectivity for ions at 50–60% loading decreases with increasing ionic size and hydration energy (15).

This picture is consistent with the numbers of water molecules and ions in zeolites X and Y. A unit cell of zeolite X contains 270 water molecules. Most of this water is in the large cages together with 69 cations. The numbers tell us that not all of the alkali metal cations can be fully hydrated, and X-ray crystallographic data confirm this conclusion (14). A unit cell of zeolite Y contains almost the same number of water molecules as zeolite X but contains only 34 alkali metal cations in the large cages. These cations can be fully hydrated and behave that way from an ion-exchange point of view.

Silver and thallium (I) do not fit into a selectivity series based on crystal radii or hydration energy. These cations are very polarizable because of their electronic structure. They are highly polarized by the strong electric fields within zeolites and are very tightly bound to the anionic framework. Thus, the isotherms for $Ag^+$ and $Tl^+$ exchange of $Na^+$ in zeolites X and Y shown in Figs. 5, 6, 11, and 12 fall well above the unit selectivity line. $Tl^+$ exchange in NaY looks anomalous because only 68% loading of $Tl^+$ was achieved in zeolite Y whereas 100% loading of zeolite X is achieved. According to Pauling (15), the crystal radius of $Tl^+$ is 1.40 Å, which is too large to fit through the 2.5-Å-diameter window between the supercage and the sodalite cage. However, the cation is polarizable. It probably does not fit through the 6-ring at 25°C because of the contraction in the size of the unit cell as the SAR move changes from 2.56 for zeolite X to 5.6 for zeolite Y.

For all of the univalent ions studied, the selectivity series for zeolites X and Y at low loadings is Ag≫Tl(I) > Cs > Rb > K > Na  Li.

Studies of alkylammonium ion exchange of zeolites NaX and NaY (19) support the hypothesis that complete replacement of $Na^+$ by $Rb^+$ and $Cs^+$ ions in the large cage of zeolite X is not possible due to the large volume of these cations—a crowding effect. This study showed that in ion exchange involving alkylammonium ions the maximal extent of exchange decreases with increasing molecular weight. This result is consistent with the volume requirements of the incoming organic cations.

### B. Di-Univalent Ion Exchange

A comprehensive study of alkaline earth ion exchange in zeolites X and Y over the temperature range of 5°–50°C was made by Sherry (7). Barrer et al. reported on alkaline earth ion exchange of zeolite X at 25°C (10). Barrer et al. reported on zeolite Y at 25°C (8). The ion-exchange isotherms for $Ca^{2+}$, $Sr^{2+}$, and $Ba^{2+}$ ion exchange of zeolites X and Y at 0.1 total normality of chloride solution, taken from Sherry (7), are presented in Figs. 14–24. These isotherms show that 100% exchange is not achieved in all cases. Complete exchange of NaX was achieved by $Ca^{2+}$ and $Sr^{2+}$ at 25°C and 50°C (Figs. 14–17) and with $Ba^{2+}$ at 50°C (Fig. 19). The solid line in Fig. 14 is a $Ca^{2+}$-$Na^+$ ion exchange isotherm obtained using 1 h of exchange time at 25°C. It shows that only 82% exchange occurs at short contact times. Sherry (7) reported that at 5°C and 25°C when

Copyright © 2003 Marcel Dekker, Inc.

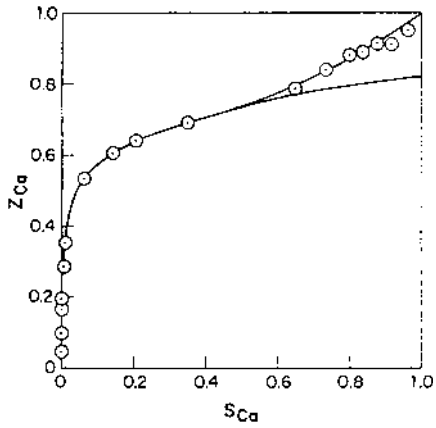


**Fig. 14** The ion-exchange isotherm for the Ca-Na-X system at 25°C and 0.100 total normality. (From Ref. 7.)

a 1000-fold excess of $Ba^{2+}$ is used only 82% of the $Na^{+}$ can be replaced from NaX over 4 weeks. Only 68% of the $Na^{+}$ in NaY can be replaced by $Ca^{2+}$, $Sr^{2+}$, or $Ba^{2+}$ ions in a reasonable time (Figs. 20–24) at temperatures up to 50°C.

The inability of $Ba^{2+}$ to exchange the $Na^{+}$ in the network of small cages of zeolite X at 25°C can be attributed in part to the ionic radius of the bare ion being 1.35 Å (15). However, $K^{+}$ ions, with an ionic radius of 1.33 Å (15), diffuse rapidly into the small cages of zeolite X. Increasing the temperature to 50°C permits $Ba^{2+}$ ions to rapidly penetrate the sodalite cages. We hypothesize that three factors contribute to the replacement of $Na^{+}$ by $Ba^{2+}$ in the network of small cages at 50°C:

1. The increase in temperature supplies energy of dehydration.
2. The increase in temperature provides additional kinetic energy for diffusion of the bare ions into the sodalite cages.
3. The increase in temperature causes greater vibration of the aluminosilicate framework.

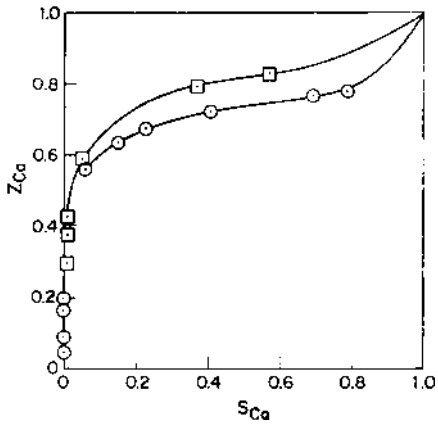


**Fig. 15** The ion-exchange isotherm for the Ca-Na-X system at 50°C. ○, 0.103 total normality; □, 0.050 total normality. (From Ref. 7.)

Copyright © 2003 Marcel Dekker, Inc.

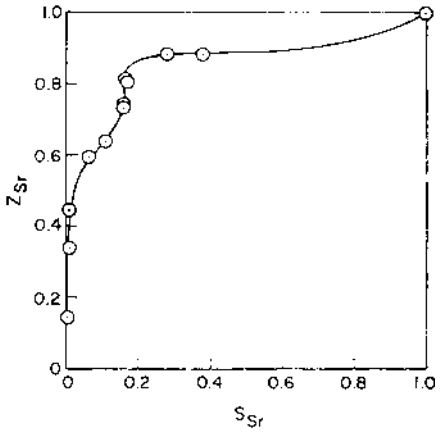


**Fig. 16** The ion-exchange isotherm for the Sr-Na-X system at 25°C and 0.100 total normality. (From Ref. 7.)

The isotherms for Sr-Na-X at 25°C and 50°C (Figs. 16 and 17) have a very unusual shape. Close inspection shows that there is a region of these curves where the zeolite phase varies in composition at constant composition of the solution phase. This result appears to violate the phase rule. An X-ray powder diffraction study by Olson and Sherry (17) shows that when $Sr^{2+}$ ions are exchanged into NaX the cubic unit cell contacts. At 71% Sr loading, the unit cell suddenly expands and a new phase forms that is richer in Sr than the original phase. This data explain the unusual ion-exchange isotherm found for the Sr-Na-X system. The ion-exchange isotherm shown in Fig. 16 has a sudden vertical rise at about 70% Sr loading because a new Sr-rich phase forms that that is not miscible in the old Sr-poor phase. These two phases are not miscible in each other because the Sr-rich phase has a significantly larger unit cell size than the Sr-poor phase. Over the range of $Sr^{2+}$ ion

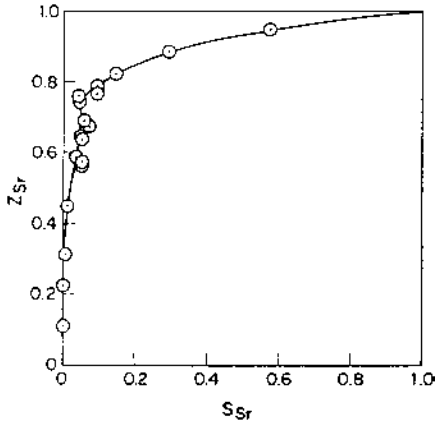


**Fig. 17** The ion-exchange isotherm for the Sr-Na-X system at 50°C and 0.100 total normality. (From Ref. 7.)

Copyright © 2003 Marcel Dekker, Inc.

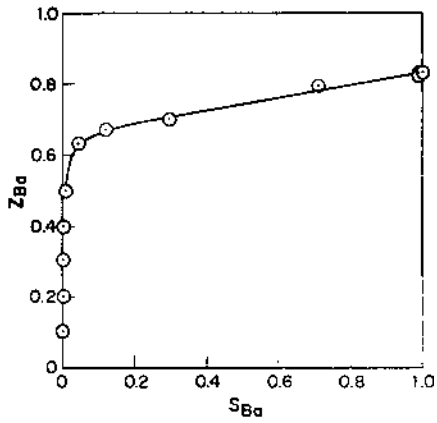


**Fig. 18** The ion-exchange isotherm for the Ba-Na-X system at 25°C and 0.100 total normality. (From Ref. 7.)

loading from 71% to 87% the new phase grows at the expense of the old phase until finally the Sr-poor phase disappears.

The Sr-Na-X system is not the first example of limited miscibility of end members. Barrer and Hinds (18) reported that $K^+$ ion exchange of Na-analcite converts some of the crystals to K-leucite at low levels of K loading. The two-solid phase region extends over almost the complete range of ion exchange. Two solid phases were also obtained in the Tl-Na-, Rb-Na-, Tl-K-, and Ag-Na-analcite systems (18). It would appear that almost complete immiscibility of end members occurs when a large ion replaces a small one in a zeolite that has a fairly dense framework structure. The Sr-Na-X system is more complicated. Olson and Sherry (17) have shown that in the new, Sr-rich, expanded phase the cation sites in the hexagonal prisms are empty, whereas in the Sr-poorer phase they are almost completely occupied by $Na^+$. The loss of positive charge in the hexagonal prisms may cause the O atoms to move apart, resulting in a large expansion of the unit cell.

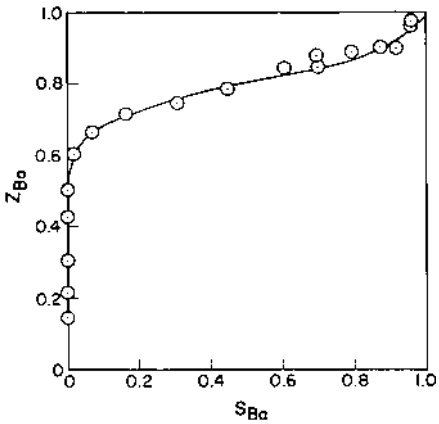


**Fig. 19** The ion-exchange isotherm for the Ba-Na-X isotherm at 50°C and 0.1 total normality. (From Ref. 7.)

Copyright © 2003 Marcel Dekker, Inc.

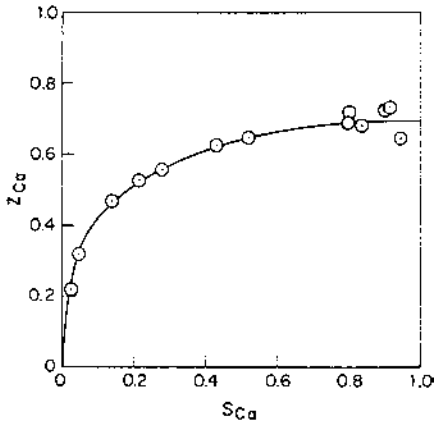


**Fig. 20** The ion-exchange isotherm for the Ca-Na-Y system at 25°C and 0.1 total normality. (From Ref. 7.)

Despite all the complexities of phase transition and sieving of large cations from the small cages, below 50% loading the alkaline earth ion selectivity series is $Ba^{2+} > Sr^{2+} > Ca^{2+}$. The selectivity decreases with decreasing size and increasing dehydration energy of the hydrated ion.

## C. Rare Earth Ion Exchange

In 1969, Sherry (20) reported on rare earth ion exchange in zeolites NaX and NaY. The isotherms are shown in Fig. 25. The most important result of this work was to show that $La^{3+}$ ions cannot easily replace the $Na^{+}$ ions that are in the network of small cages of zeolites X and Y. The isotherms for La-Na-X and La-Na–Y systems, obtained at 25°C, terminate at 85% and 68% exchange, respectively. At higher temperatures there is a very slow replacement of the $Na^{+}$ in the network of small cages by $La^{3+}$. The isotherms obtained at 82.2°C show that a small amount of the $Na^{+}$ in the small cages is replaced in a reasonable amount of time. The ion-exchange reaction can be accelerated by the use of

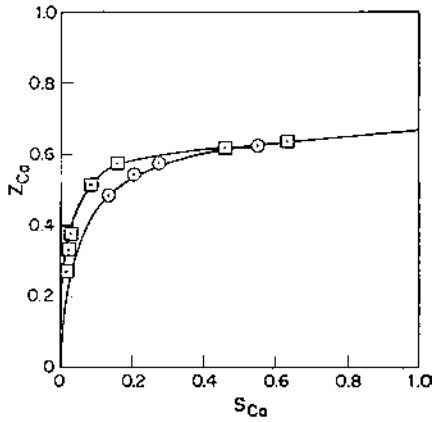


**Fig. 21** The ion-exchange isotherms for the Ca-Na-Y system at 50°C. ○, 0.103 total normality; □, 0.051 total normality. (From Ref. 7.)

Copyright © 2003 Marcel Dekker, Inc.

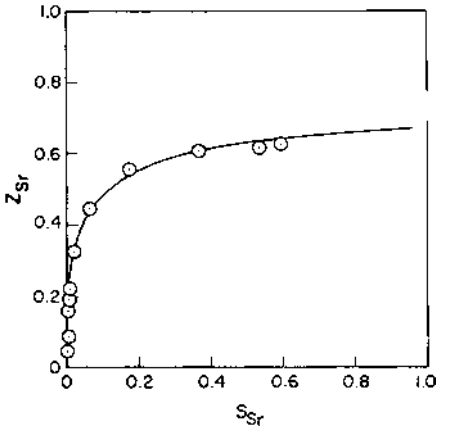


**Fig. 22** The ion-exchange isotherm for the Sr-Na-Y system at 50°C and 0.100 total normality. (From Ref. 7.)

very high temperatures under autogenous pressure (21). But high-temperature ion exchange using rare earth chloride solution under autogeneous pressure is not simple. Sherry and Schwartz (21) showed that, at the pH of rare earth chloride solutions and the temperatures required to accomplish appreciable replacement of the $Na^+$ in the small cages at a reasonable rate, appreciable crystallinity can be lost. They showed that at sufficiently high temperature the ion-exchange reaction is much faster than the reactions that are responsible for loss of crystallinity. Therefore, high temperatures and short contact times are recommended (21).

A more convenient method for preparing low-Na rare earth X or Y was described by Sherry (22). He showed that at 25°C the following process produces a low-Na rare earth X or Y:

1. Ion exchange with 0.3 N $LaCl_3$ at 25°C to replace all or most of the $Na^+$ in the large cages.

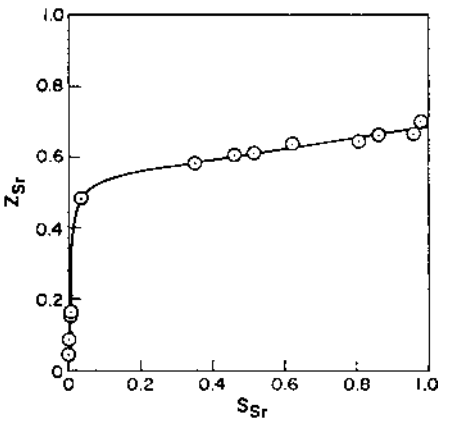


**Fig. 23** The ion-exchange isotherm for the Sr-Na-Y system at 25°C and 0.100 total normality. (From Ref. 7.)

Copyright © 2003 Marcel Dekker, Inc.

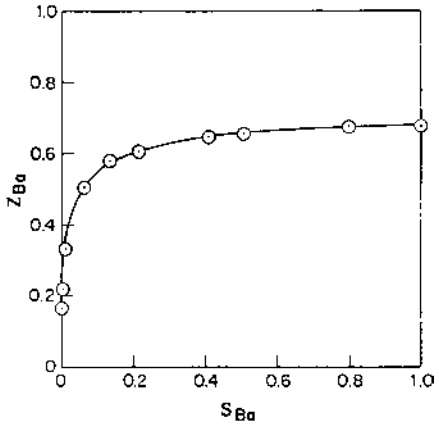


**Fig. 24** The ion-exchange isotherm for the Ba-Na-Y system at 25°C and 0.100 total normality. (From Ref. 7.)

2. Calcine the product of the first step at 370° for 40 min or at 482°C for 20 min.
3. Re-exchange the product of the second step with 0.3 N $LaCl_3$ to replace the remaining $Na^+$ ions.

Sherry (22) described the phenomenon that takes place in the second step as an intercage exchange of $Na^+$ and $La^{3+}$ ions. When the water molecules in the large cages are removed during calcination, $La^{3+}$ ions diffuse into the sodalite cages and $Na^+$ ions diffuse into the large cages where they are readily replaced by $La^{3+}$ in the third step. Sherry also showed (22) that after calcination the rare earth cations from step 1 are not exchangeable and cited evidence that they form a very stable complex with a water molecule and oxygen atoms in the sodalite cages. The results of this three-step process are

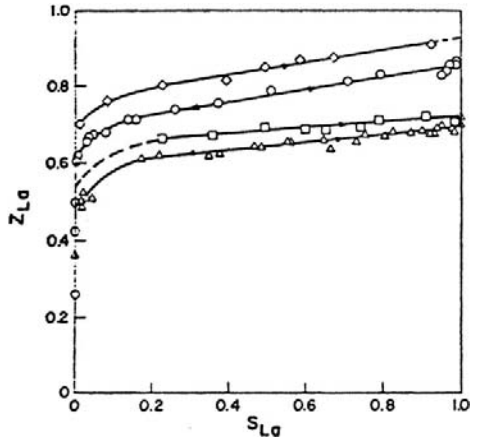


**Fig. 25** The ion-exchange isotherms for the La-Na-X and La-Na-Y systems at 0.3 total normality and at 25°C and 82.2°C using LaCl3. ○, $La_s^{3+} + 3NaX \leftrightarrow LaX_3 + 3Na_s^+$ at 25°C; Δ, $La_s^{3+} + 3NaY \leftrightarrow LaY_3 + 3Na_s^+$ at 25°C; ◇, $La_s^{3+} + 3NaX \leftrightarrow LaX_3 + 3Na_s^+$ at 82.2°C; □, $La_s^{3+} + 3NaY \leftrightarrow LaY_3 + 3Na_s^+$ at 82.2°C. (From Ref. 20.)

Copyright © 2003 Marcel Dekker, Inc.

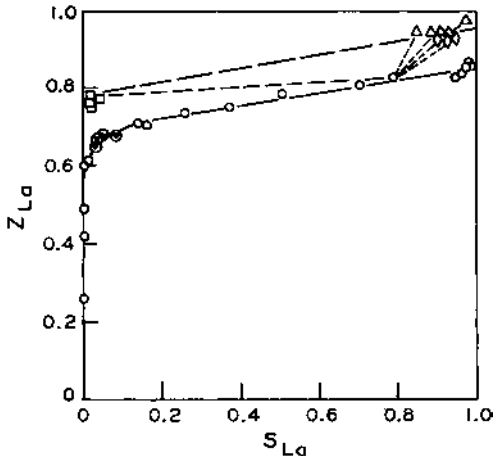


**Fig. 26** The effect of heating on the ion-exchange properties of $La_{82}Na_{18}X$ at 25°C and 0.3 total normality of $LaCl_3$. ○, $La^{3+}$ + 3NaX (not dried or dried ); ∇, 3Na+ + $La_{82}Na_{18}X$ (not dried); Δ, $La^{3+}$ + $La_{82}Na_{18}X$ (dried at 121°C for 24 h);◇, $La^{3+}$ + $La_{82}Na_{18}X$ (dried at 425°C for 15 min); □, $3Na^{+}$ + $La_{82}Na_{18}X$ (dried at 121°C for 24 h). (From Ref. 22.)

illustrated in Figs. 26 and 27. This technique of exchange, calcine, and re-exchange to produce low-Na zeolites X and Y will work with other cations provided that the inhibition to replacement of $Na^{+}$ in the small cages is not due to the bare ion size of the ingoing cation. Rare earth cations are much smaller than the opening into the sodalite cages (15). Thus, it is the size of the hydrated ion that inhibits movement into the small cages in the first step.

In this same study (22), it was shown that any combination of time and temperature of calcination in the second step that removes water molecules allows the third step to be accomplished. It was shown that the rare earth cations present in the first step are not

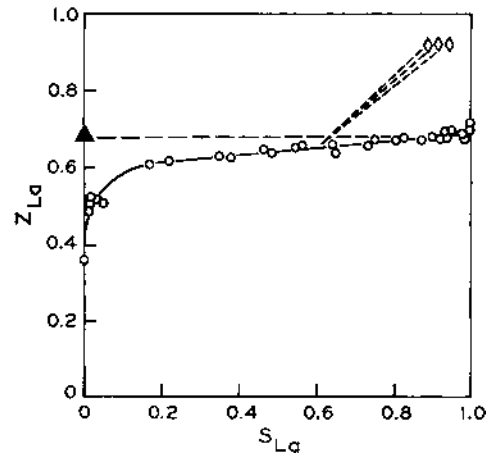


**Fig. 27** The effect of heating on the ion-exchange properties of $La_{66}Na_{34}Y$ at 25°C and 0.3 total normality. ○, La3+ + 3NaY (not dried or dried);◇, $La^{3+}$ + $La_{66}Na_{34}Y$ (dried at 121°C for 24 h); ▲, 3Na+ + $La_{66}Na_{34}Y$ (dried at 121°C for 24 h). (From Ref. 22.)

Copyright © 2003 Marcel Dekker, Inc.

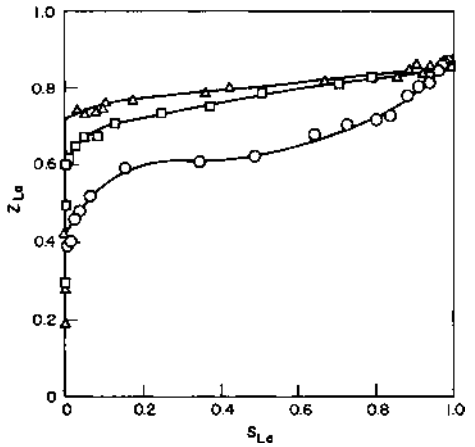


**Fig. 28** The effect on the LaNaX system of varying total normality at 25°C. Δ, 0.06 total normality; □, 0.3 total normality; ○, 3.85 total normality. (From Ref. 20.)

exchangeable in the third step. They are fixed in the structure most probably due to the stability of the bonds to framework and water oxygen atoms in the sodalite cages. Even exhaustive ion exchange with ammonium salt solutions could not re-exchange these rare earth cations. A direct correlation between the number of water molecules removed per unit cell in the second step and the number of rare earth cations that are fixed was demonstrated in Ref. 22.

Rare earth ion exchange enables us to demonstrate the "electroselective effect." The effect is illlustrated in Fig. 28 where the isotherms for the La-Na-X system are shown at 0.06, 0.30, and 3.85 total normality of chloride solution at 25°C. It can be seen that the selectivity of $La^{3+}$ over $Na^{+}$ decreases with increasing total normality. The statement of the Electoselectivity effect is that when the ingoing ion is more highly charged than the outgoing ion, the preference for the ingoing ion decreases with increasing solution normality. The converse is also true. Increasing the total normality favors the lower charged ion.

## IV. ION EXCHANGE IN ZEOLITE A

### A. Uni-Univalent Exchange

The framework structure and most of the cation positions are known for hydrated zeolite NaA (13). Zeolite A is formed by stacking sodalite cages. However, instead of being joined through adjacent 6-rings to form hexagonal prisms as is the case for zeolites with the faujasite structure, they are joined through adjacent 4-rings to form square prisms. The sodalite cages stack in a simple cubic array with a large cage in the center of the cube (Fig. 29). The entrance to the large cage is an 8-ring with a free diameter of 4 Å. The window between the large cage and sodalite cage is a 6-ring with a free diameter of 2.5 Å. There are 12 $Na^{+}$ per unit cell, all in the one large cage per unit cell. Eight are located near the center of the 6-rings separating the large and small (sodalite) cages, one near the center of each of the eight 6-rings per unit cell. The other four Na atoms have not been located and they are assumed to be dissolved in the zeolitic water in the large cages.

Copyright © 2003 Marcel Dekker, Inc.

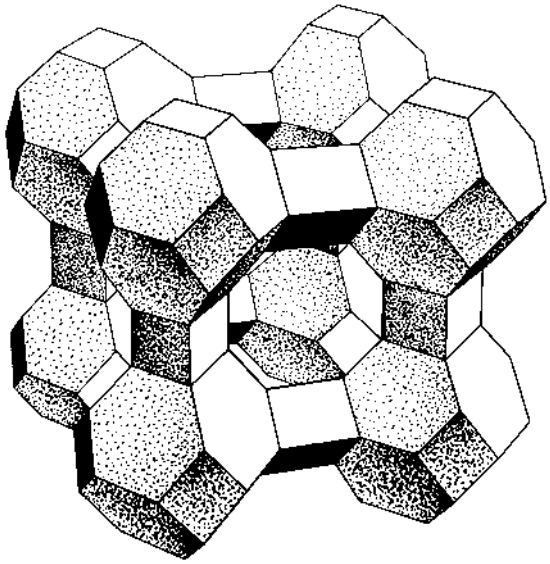

**Fig. 29** Zeolite A structure. (From Ref. 44.)

Barrer and Falconer (25) and Barrer and Meier (26) studied $Li^+$, $K^+$, $Rb^+$, and $Cs^+$ ion exchange of NaA. Their results are not much different than what was obtained with NaX as far as the isotherm shapes and the selectivity series.

Both Sherry (27) and Barrer and coworkers (25,26) reported that zeolite A, which has a SAR of 2, has a very high selectivity for $Ag^+$ and $Tl^+$ ions—even higher than does zeolite X. Ion exchange isotherms are shown in Figs. 30 and 31.

## B. Di-Univalent Ion Exchange

Ion-exchange isotherms for the Ca-Na-A, Sr-Na-A, and Ba-Na-A systems (27) are shown in Figs. 32–34. These isotherms lie farther above the unit selectivity line than those for

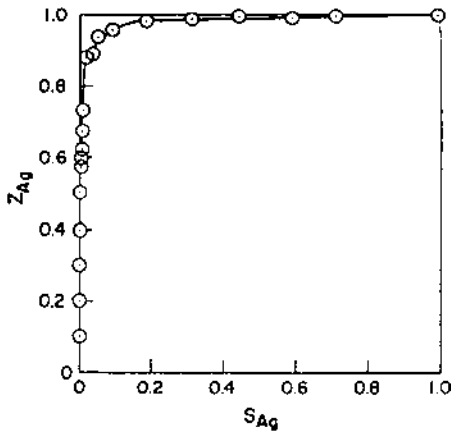


**Fig. 30** The ion-exchange isotherm for the Ag-Na-A system at 0.1 total normality and 25°C. ○ $Ag_s^+ + Na_z^+$. (From Ref. 27.)

Copyright © 2003 Marcel Dekker, Inc.

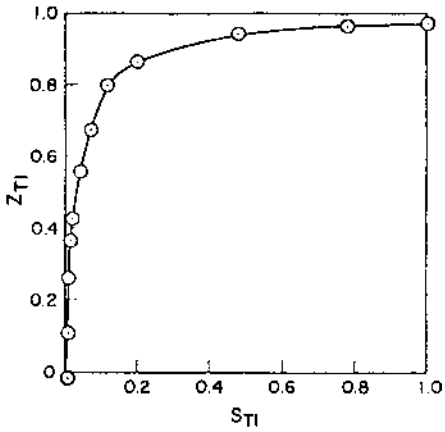


**Fig. 31** The ion-exchange isotherm for the Tl-Na-A system at 0.1 total normality and 25°C. ○, $Tl_s^+ + Na_z^+$. (From Ref. 27.)

zeolite X, indicating that zeolite NaA is even more selective for alkaline earth ions than zeolite NaX. Again, the selectivity series is $Ba^{2+} > Sr^{2+} > Ca^{2+}$. Thus , the least hydrated ion is most preferred. We will show later in the section on the thermodynamics of ion exchange that the explanation for this selectivity series lies in both the zeolite and the solution phase.

A study of $Cd^{2+}$ and $Pb^{2+}$ ion exchange of NaA has been reported (28). This work showed that zeolite NaA is extremely selective for these two heavy cations. The isotherms are shown in Figs. 35 and 36. Just as in the case of $Ag^+$ and $Tl^+$, the cause of the high selectivity lies in the polarizability of these divalent cations by the strong electric fields within the zeolite crystals.

Figure 36 shows that overexchange of $Cd^{2+}$ occurred when $Cd(CH_3COO)_2$ is used instead of $Cd(NO_3)_2$. This is undoubtedly due to the partial hydrolysis of $Cd^{2+}$ to form $Cd(OH)^+$ resulting from the use of the basic acetate anion. Later work (29) demonstrated the occurrence of Pb overexchange in zeolites NaX and NaY.

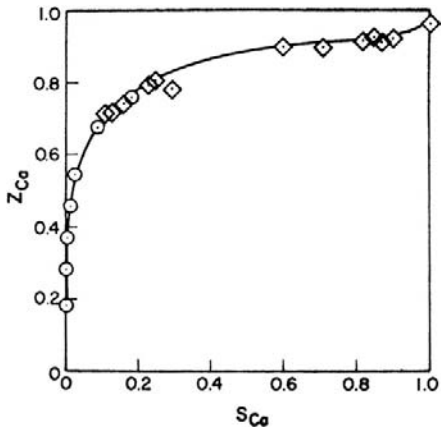


**Fig. 32** The ion-exchange isotherm for the Ca-Na-A system at 0.1 total normality and 25°C. ○, $Ca_s^{2+} + 2Na^+$, radioactive tracer used; ◇, $Ca_s^{2+} + 2Na^+$, no radioactive tracer used. (From Ref. 27.)

Copyright © 2003 Marcel Dekker, Inc.

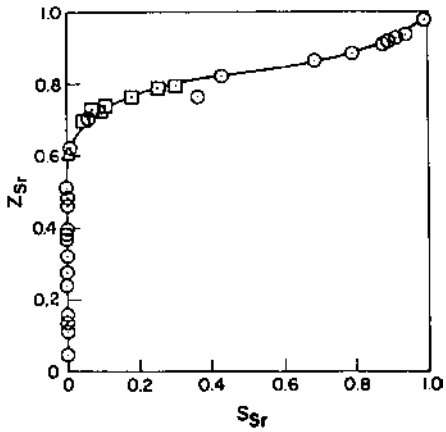


**Fig. 33** The ion-exchange isotherm for the Sr-Na-A system at 0.1 total normality and 25°C. ○, $Sr_s^{2+} + 2Na_z^+$, no radioactive tracer used; □, $2Na_s^+ + Sr_z^{2+}$, no radioactive tracer used; Δ, $Sr_s^{2+} + 2Na^+$, radioactive tracer used. (From Ref. 27.)

## V. ION EXCHANGE IN SOME SYNTHETIC AND NATURAL ZEOLITES WITH INTERMEDIATE SAR

### A. Ion Exchange in Zeolite T and Erionite

Thus far, we have considered zeolites with low SARs ranging from 2.0 for zeolite A to 5.6 for zeolite Y. More siliceous zeolites are expected to have different ion selectivities. Sherry (30) has studied univalent and divalent ion exchange in the synthetic zeolite T, a zeolite with a SAR of 7. This zeolite is essentially a synthetic version of the natural zeolite, offretite, with small intergrowths of erionite (31). The offretite structure (Fig. 37) is capable of exhibiting ion-sieving effects because it has two networks of channels. The more open network consists of channels with 12-ring openings having an effective diameter of

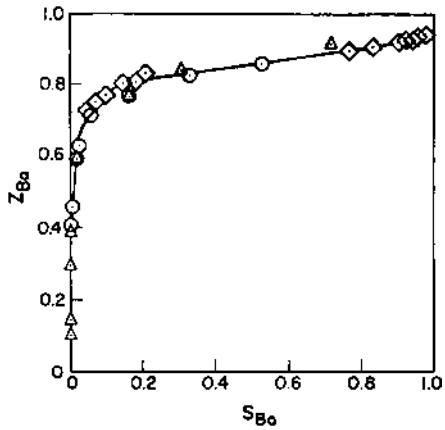


**Fig. 34** The ion-exchange isotherm for the Ba-Na-A system at 0.1 total normality and 25°C. ○, $Ba_s^{2+} + 2Na_z^+$, no radioactive tracer used; □, $2Na_s^+ + Ba_z^{2+}$, no radioactive tracer used; Δ, $Ba_s^{2+} + 2Na^+$, radioactive tracer used. (From Ref. 27.)

Copyright © 2003 Marcel Dekker, Inc.

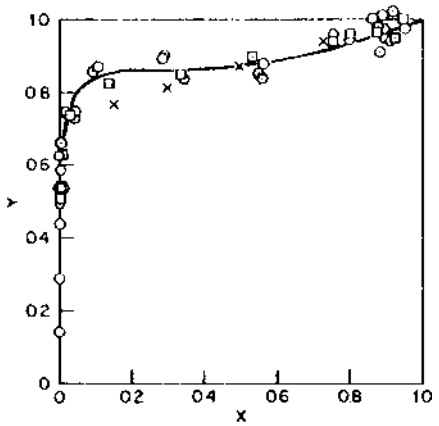


**Fig. 35** $CdNO_3$-Na-A system at 0.1 total normality. ○, $NO_3^-$ at 5°; □, at 25°C; $NO_3^-$; ⬭, $NO_3^-$ at 50°C; x, $Cl^-$ at 25°C. (From Ref. 28.)

6.7 Å for spherical cations. These channels do not intersect and run parallel to the *c* axis of the hexagonal unit cell. A denser network consists of columns of alternating cancrinite cages and hexagonal prisms. These columns are also parallel to the *c* axis and link together to form columns of gmelinite cages and the long column bounded by 12-rings. The gmelinite cages open into the large channels via 8-rings with an effective diameter of 3.6 Å. The window into the cancrinite cage is a very puckered 6-ring having a limiting dimension of 1.76 Å. The long open channel is randomly blocked by intergrowths of erionite. The offretite structure is shown in Fig. 37.

Exhaustive ion exchange of a batch of KT having an anhydrous unit cell composition of $K_4[(AlO_2)_4(SiO_2)_{14}]$ with $Cs^+$, $Rb^+$, $Ca^{2+}$, $Ba^{2+}$, and $NH_4^+$ showed that only three of the four $K^+$ ions in a unit cell could be replaced (27). One was not exchangeable. It was concluded that, because of the size of the $K^+$ ion (Pauling diameter of 2.66 Å) (15), one was trapped in the one cancrinite cage in a unit cell during synthesis. The exchange-

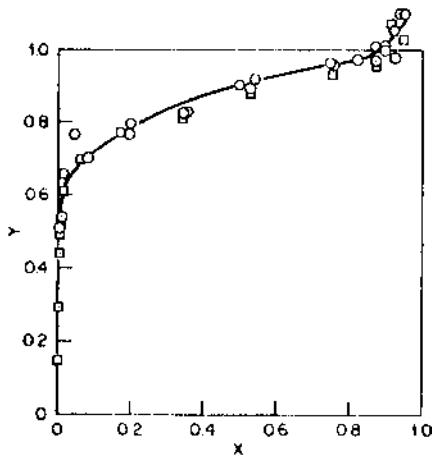


**Fig. 36** $Cd(CH_3COO)_2$ -Na-A system at 0.1 total normality. ○, $NO_3^-$ at 5°C; □, at 25°C; $NO_3^-$; ⬭ $NO_3^-$ at 50°C. (From Ref. 28.)

Copyright © 2003 Marcel Dekker, Inc.

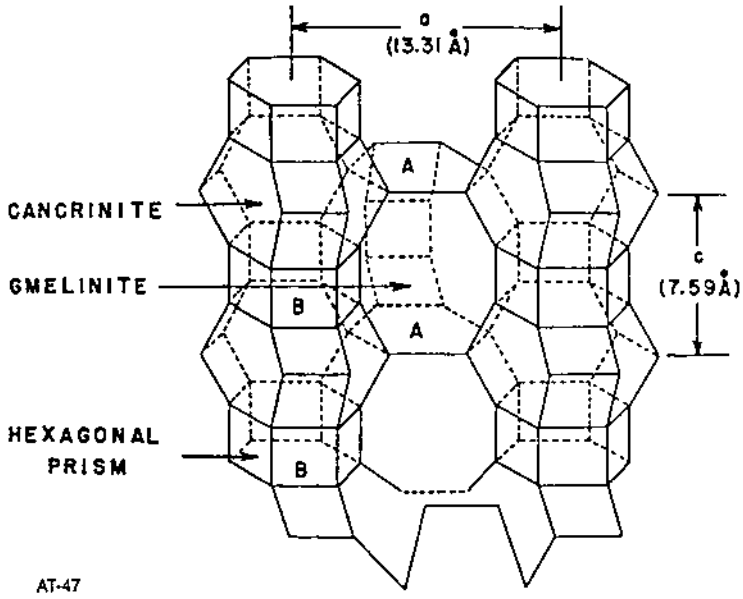


**Fig. 37** Offretite framework structure. (From Ref. 30.)

able $K^+$ in a batch of zeolite T was replaced by $Na^+$ to produce a zeolite with the anhydrous formula of $Na_3K[(AlO_2)_4(SiO_2)_{14}]$. This zeolite and the pure K form were used to obtain the isotherms shown in Figs. 38–44. In these figures 100% exchange means replacement of the three exchangeable ions per unit cell. These isotherms show that NaT is very selective for $K^+$, $Rb^+$, and $Cs^+$ and much more so than was found for zeolites NaA and NaX. The selectivity of $Ca^{2+}$ is considerably less than was found for NaA and NaX. NaT is selective for $Ag^+$ but less so than NaA and NaX.

The structure of the natural zeolite erionite is closely related to that of offretite, which is why the two zeolites can intergrow. The ion-exchange properties of natural erionite have also been studied (32). After exhaustive $Na^+$ ion exchange, the zeolite has an idealized anhydrous unit cell composition of $Na_6K_2[(AlO_2)_8(SiO2)_{28}]$. It has twice the unit cell size of offretite and therefore has two cancrinite cages in a unit cell, and it was concluded that the unexchangeable $K^+$ were in the two cancrinite cages in a unit cell. This zeolite shows selectivities for alkali metal and alkaline earth cations that are very similar to those of offretite (Figs. 45–50). Again, 100% exchange represents replacement of all of the exchangeable ions.

## B. Chabazite

Ion exchange of chabazite from Bowie, Arizona was studied by Dyer and Zubair (33). Their results are very similar to those obtained by Sherry for erionite (32). Cesium is strongly preferred over sodium and also strongly preferred over calcium and magnesium, resulting in very rectangular ion-exchange isotherms. This zeolite had a 4.1 SAR.

## C. Clinoptilolite

An ion-exchange study of clinoptilolite with an SAR of 8.34 (34) showed that ammonium ion is preferred over sodium and that sodium was preferred over the divalent cations zinc,

Copyright © 2003 Marcel Dekker, Inc.

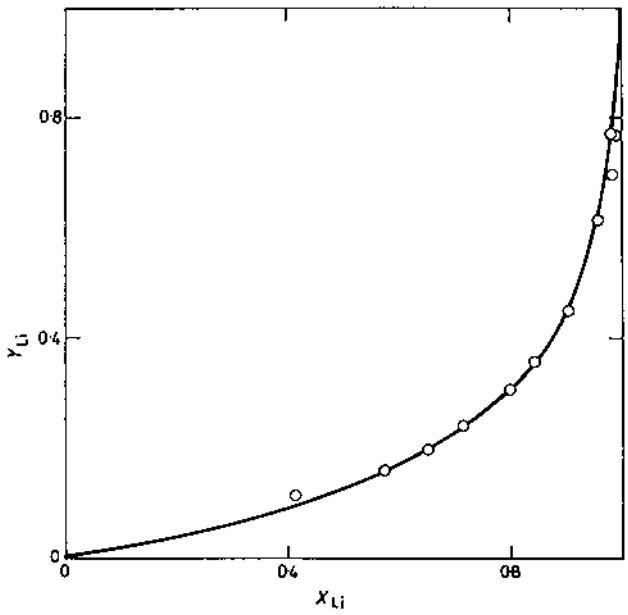


**Fig. 38** Na-Li-T ion-exchange isotherm at 0.1 total normality and 25°C. ○, $Li_s^+ + Na_z^+$. (From Ref. 30.)

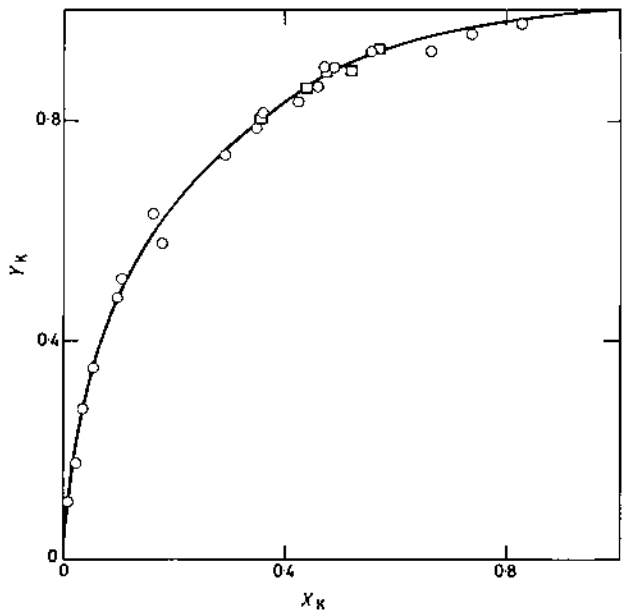


**Fig. 39** Na-K-T ion-exchange isotherm at 0.1 total normality and 25°C. ○, $Na_s^+ + K_z^+$. (From Ref. 30.)

Copyright © 2003 Marcel Dekker, Inc.

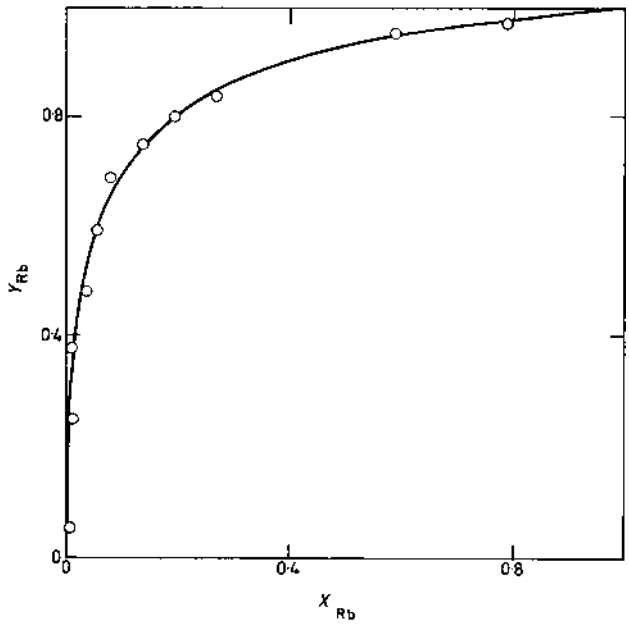


**Fig. 40** Rb-Na-T ion-exchange isotherm at 0.1 total normality and 25°C. ○, $Rb_s^+ + Na_z^+$. (From Ref. 30.)

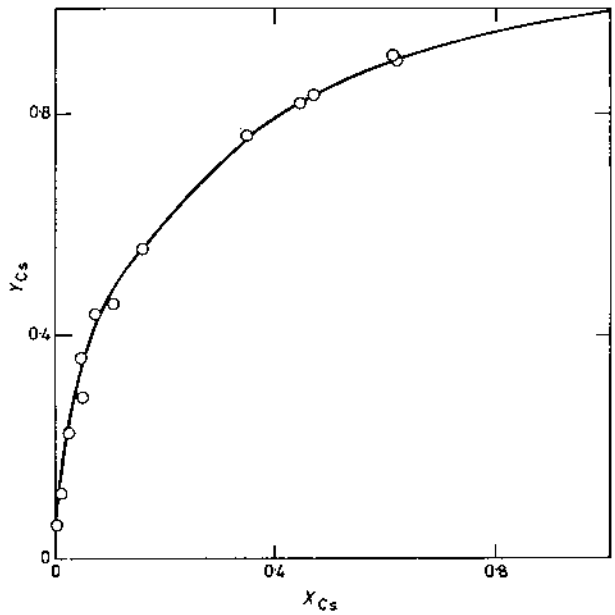


**Fig. 41** Cs-K-T ion-exchange isotherm at 0.1 total normality and 25°C. ○, $Cs_s^+ + K_z^+$. (From Ref. 30.)

Copyright © 2003 Marcel Dekker, Inc.

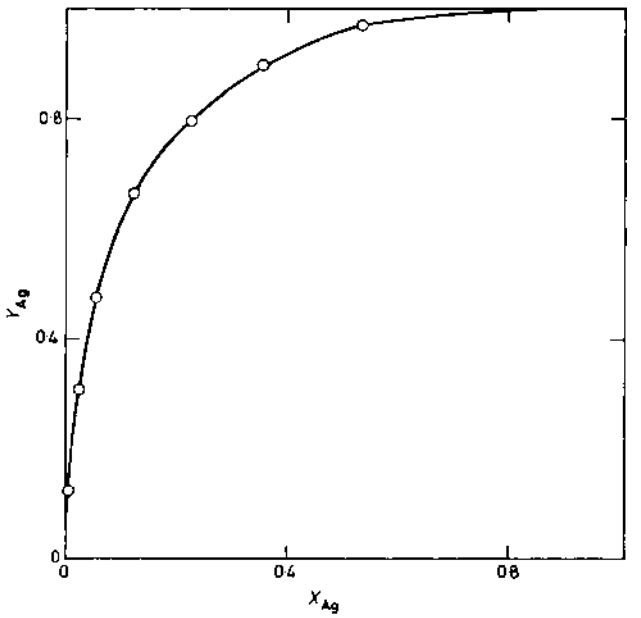


**Fig. 42** Ag-Na-T ion-exchange isotherm at 0.1 total normality and 25°C. ○, $Ag_s^+ + Na_z^+$. (From Ref. 30.)

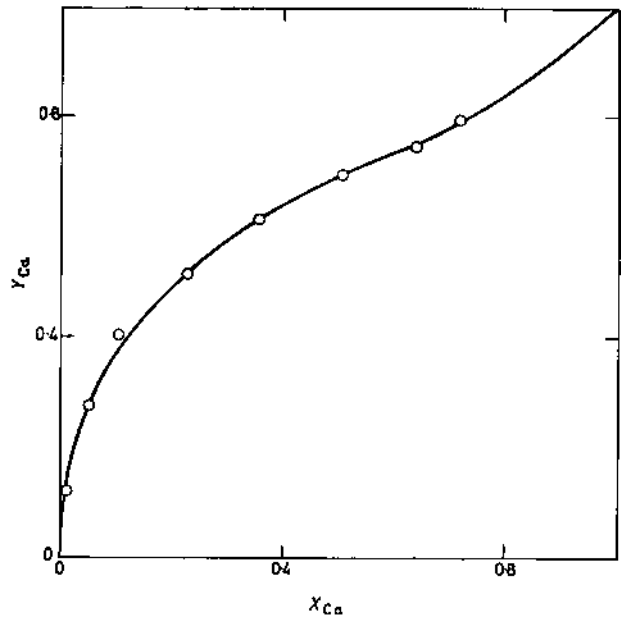


**Fig. 43** Ca-Na-T ion-exchange isotherm at 0.1 total normality and 25°C. ○, $Ca_s^{2+} + 2Na_z^+$. (From Ref. 30.)

Copyright © 2003 Marcel Dekker, Inc.

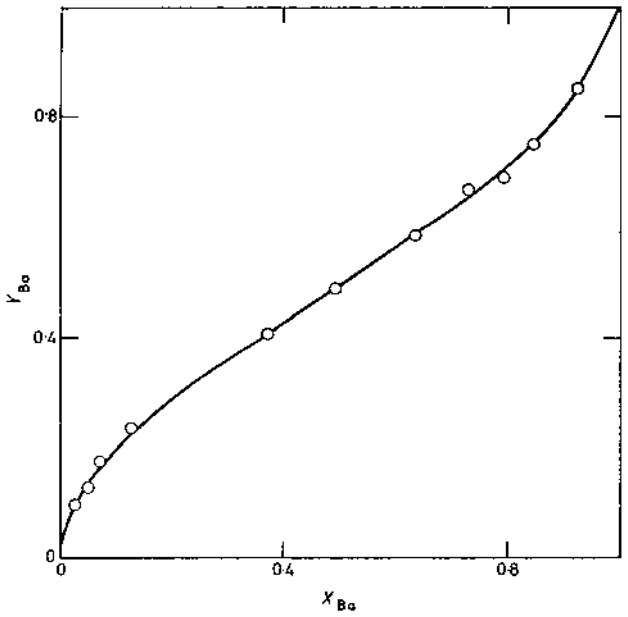


**Fig. 44** Ba-K-T ion-exchange isotherm at 0.1 total normality and 25°C. ○, $Ba_s^{2+} + 2K_z^+$. (From Ref. 30.)

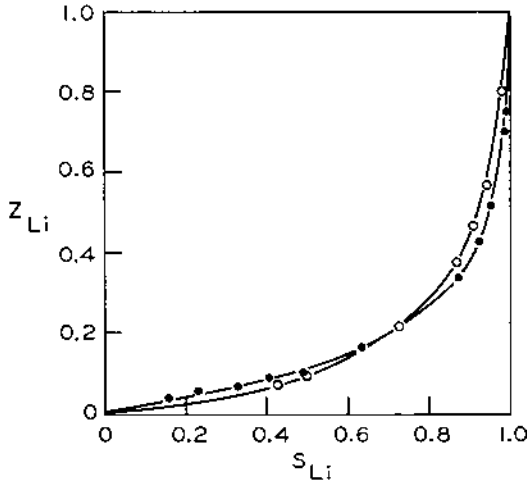


**Fig. 45** Li-Na-Erionite ion-exchange isotherm at 0.1 total normality. $Li_s^+ + Na_z^+$; ○ 25°C, ● 5°C. (From Ref. 32.)

Copyright © 2003 Marcel Dekker, Inc.

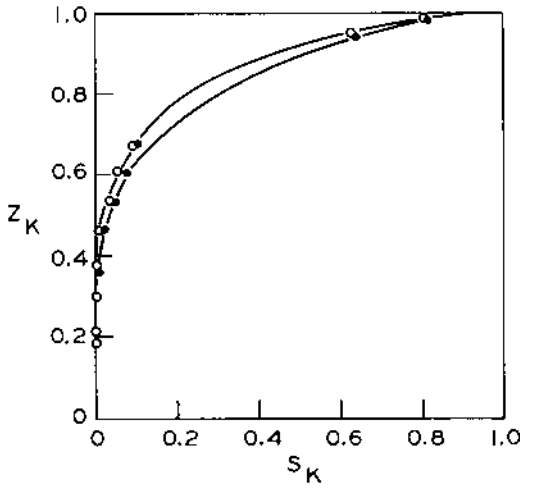


**Fig. 46** K-Na-Erionite ion-exchange isotherm at 0.1 total normality. $K_s^+ + Na_z^+$; ○ 25°C, ● 5°C. (From Ref. 32.)

copper, and cadmium. They also showed that although there was ion sieving with divalent lead it was preferred to sodium.

### D. Zeolite L

According to the structure determined by Barrer and Villiger (35), there are cations located in hexagonal prisms, in cancrinite cages, and in the main channel of this channel structure. In 1983, Newell and Rees (36) used techniques similar to those developed by Sherry (22) in 1976 to study the migration of cations from the readily exchanged sites in the main channel into sites in the hexagonal prisms and cancrinite cages and the lack of

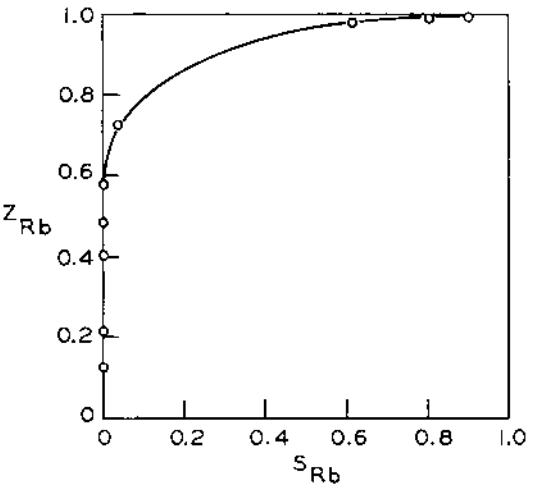


**Fig. 47** Rb-Na-Erionite ion-exchange isotherm at 0.1 total normality. $Rb_s^+ + Na_z^+$; ○ 25°C, ● 5°C. (From Ref. 32.)

Copyright © 2003 Marcel Dekker, Inc.

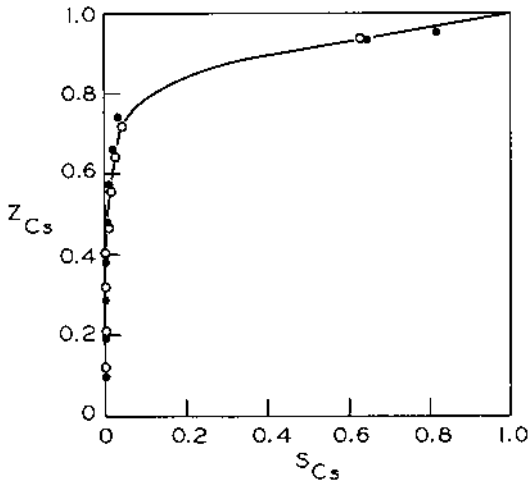


**Fig. 48** Cs-Na-Erionite ion-exchange isotherm at 0.1 total normality. $Cs_s^+ + Na_z^+$; ○ 25°C, ● 5°C. (From Ref. 32.)

exchangablity of these cations. They did this by exchanging various alkali metal, alkaline earth, and transition metal cations into the sites that were readily available for exchange—the so-called open sites. The zeolites were then calcined at various temperatures. They were exhaustively back-exchanged with ammonium chloride solutions. It was found that varying amounts of cations migrated from the open sites to the sites in the small cages. These cations were locked in and unavailable for re-exchange—another example of the irreversibility of ion exchange in a zeolite with exchange sites in large and small cages.

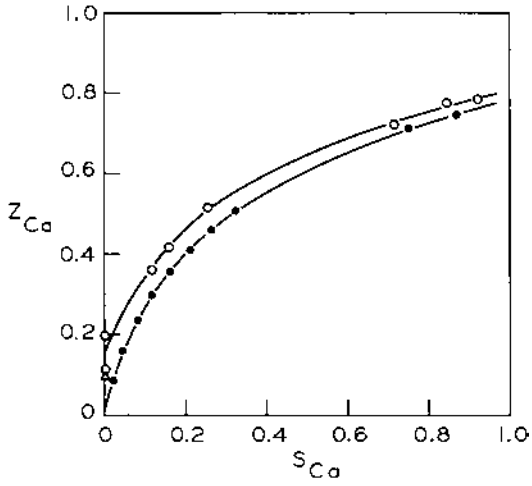


**Fig. 49** Ca-Na-erionite ion-exchange isotherm at 0.1 total normality. $Ca_s^{2+} + 2Na_z^+$; ○ 25°C, ● 5°C. (From Ref. 32.)

Copyright © 2003 Marcel Dekker, Inc.

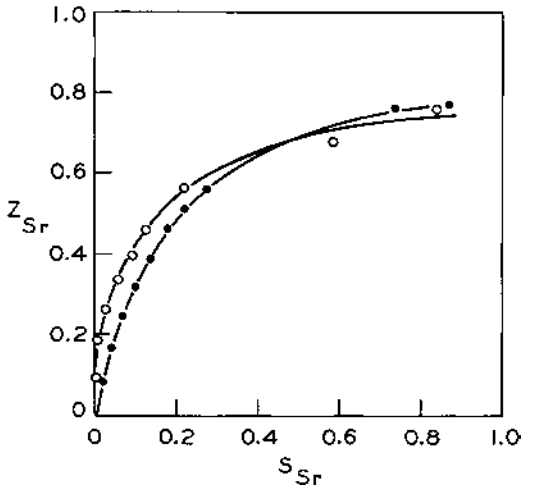


**Fig. 50** Sr-Na-erionite ion-exchange isotherm at 0.1 total normality. $Sr_s^{2+} + 2Na_z^+$; ○ 25°C, ● 5°C. (From Ref. 32.)

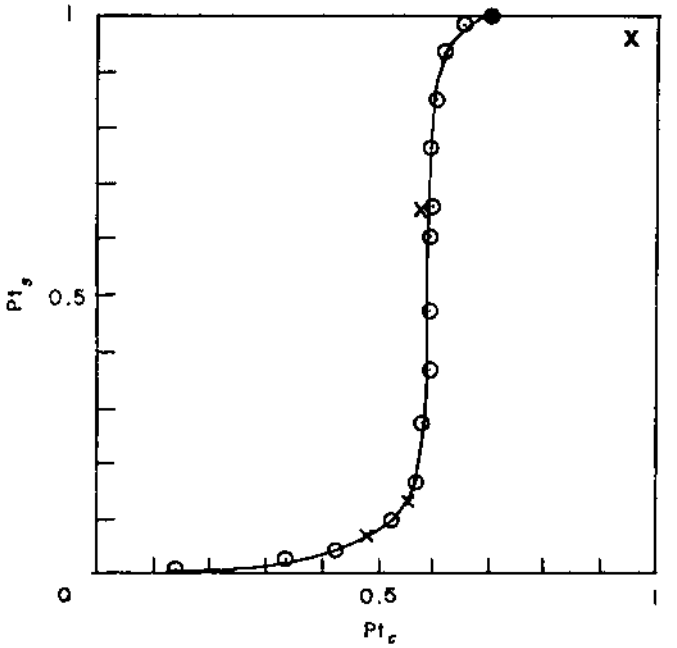


**Fig. 51** Isotherm for $[Pt(NH_3)_4]^{2+} \leftrightarrows Na^+$ exchange in X. Forward points (○), reverse points (x); direct analysis of fully exchanged solid (●). (From Ref. 37.)

Copyright © 2003 Marcel Dekker, Inc.

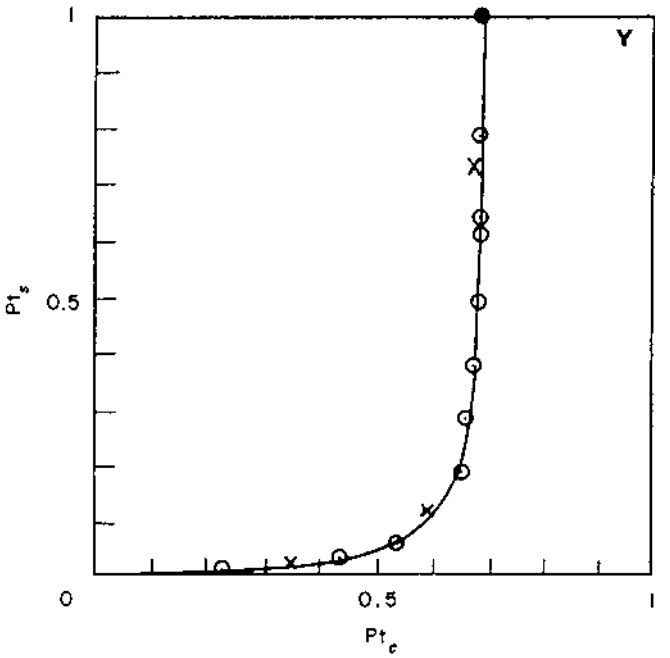


**Fig. 52** Isotherm for $[Pt(NH_3)_4]^{2+} \leftrightarrows Na^+$ in Y. (From Ref. 37.)

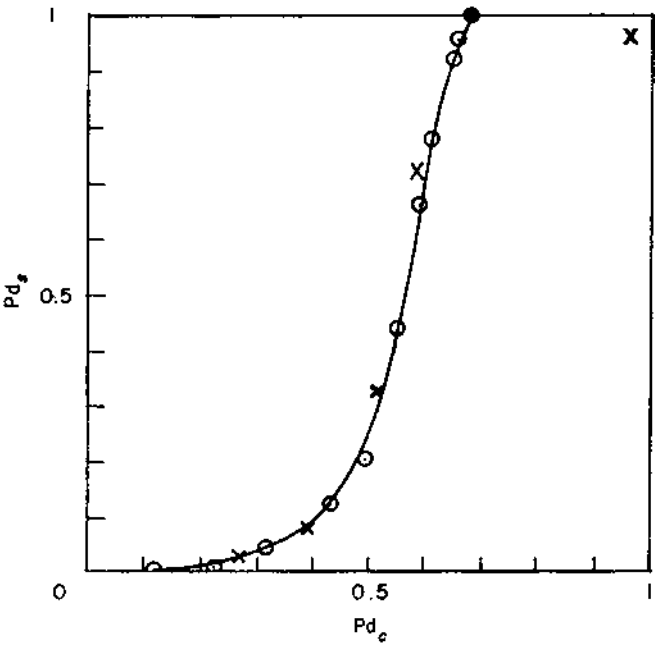


**Fig. 53** Isotherm for $[Pd(NH_3)_4]^{2+} \leftrightarrows Na^+$ in X. (From Ref. 37.)

Copyright © 2003 Marcel Dekker, Inc.

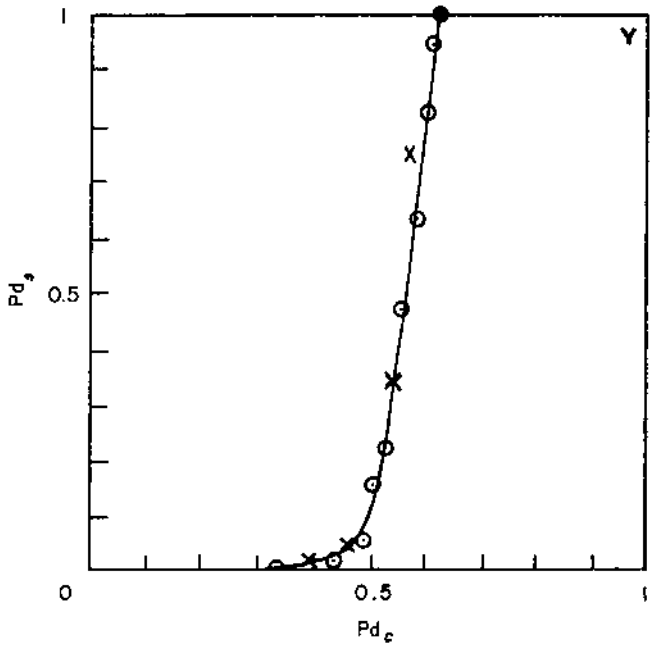


**Fig. 54** Isotherm for $[Pd(NH_3)_4]^{2+} \leftrightarrows Na^+$ in Y. (From Ref. 37.)

## VI. NOBLE METAL ION EXCHANGE IN ZEOLITES NaX, NaY, AND MORDENITE

Fletcher and Townsend (37) studied the exchange $Pt(NH_3)_4^{2+}$ and $Pd(NH_3)_4^{2+}$ ions into NaY, NaX, and NaMOR. Incomplete ion exchange of sodium was obtained with either noble metal complex cation in zeolite X, Y, and mordenite. Their ion-exchange isotherms are shown in Figs. 51–56. Figures 51–54 show that the maximal level of exchange for both Pd and Pt was about 70% in zeolite Y and and 60% in zeolite X. In the case of zeolite Y that cut-off corresponds to replacing all of the sodium cations in the supercages of the zeolite because 70% are located in the supercages. The same result was obtained with large cations like $Cs^+$ (7) and small but highly hydrated cations like $La^{3+}$ (20). The cut-off point of 60% in zeolite X indicates that these complex cations are too large to replace all of the cations in the supercages of NaX. In this zeolite 82% of the $Na^+$ are located in the supercages. Most likely when too many of the large complex cations move into the supercages of NaX they crowd out some of the sodium ions into the sodalite cages. One could look at this as a "volume effect." The same effect has been observed with ammonium alkyl exchange (38) and the exchange of amine complexes of copper(II) and silver(I).

Figures 55 and 56 show that the maximal exchange level in mordenite is 60%. Fletcher and Townsend (37) state that this result represents exchange of more than the 50% of the total $Na^+$ that are expected to reside in the main channels. The removal of more sodium than resides in the large channel of Na-mordenite indicates that loading up the large channels with platinum and palladium amine complexes causes more $Na^+$ to move from the side channels of the zeolite into the main channel.

Copyright © 2003 Marcel Dekker, Inc.

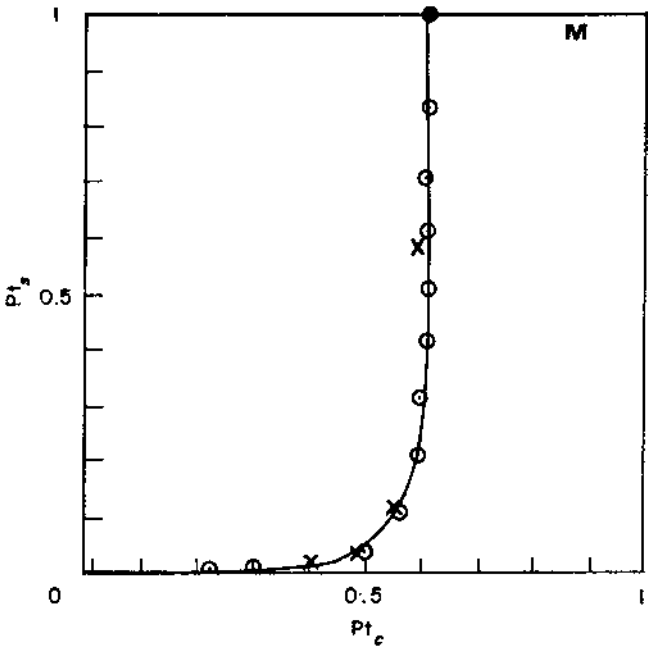


**Fig. 55** Isotherm for $[Pt(NH_3)_4]^{2+} \leftrightarrows Na^+$ in MOR. (From Ref. 37.)

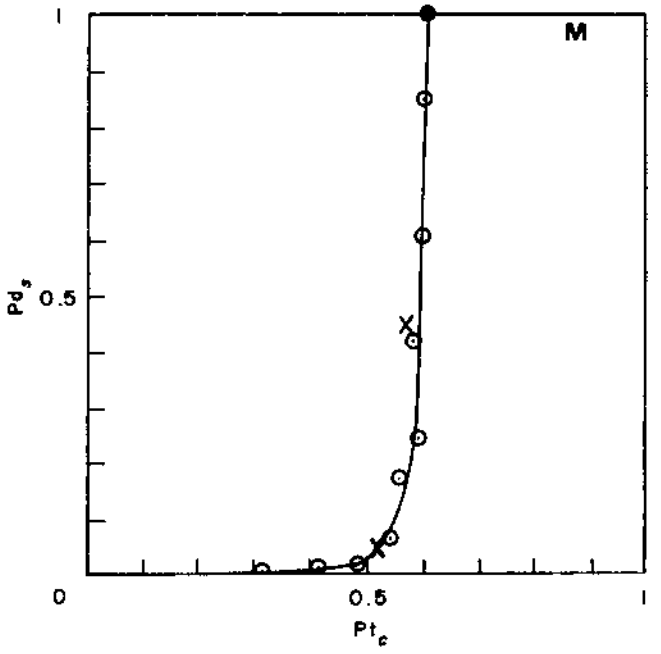


**Fig. 56** Isotherm for $[Pd(NH_3)_4]^{2+} \leftrightarrows Na^+$ in MOR. (From Ref. 37.)

Copyright © 2003 Marcel Dekker, Inc.

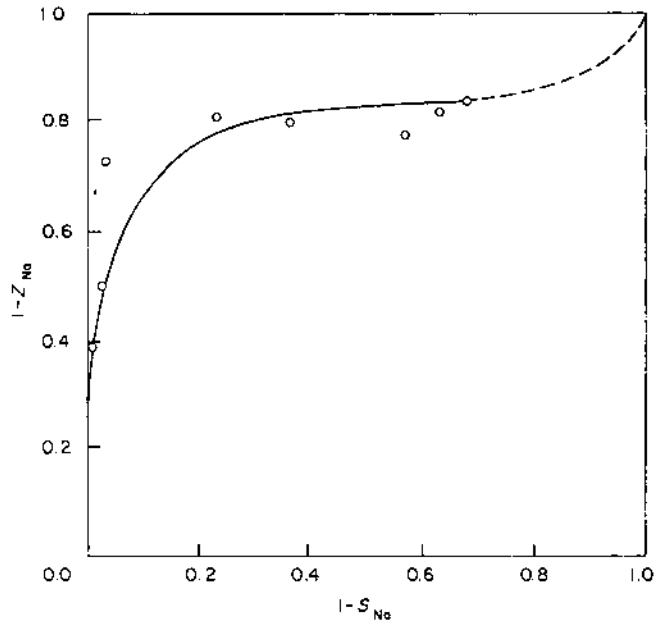


**Fig. 57** $H_3O^+$-$Na^+$ exchange isotherm of NaY using Dowex 50X8 at 25°C. (From Ref. 39.)

## VII. ION EXCHANGE OF SILICA-RICH ZEOLITES

### A. Hydronium Ion Exchange

A clever technique was used Chu and Dwyer (39) to $H_3O^+$ ion-exchange zeolites Y, mordenite, ZSM-4, ZSM-5, and ZSM-11 from very dilute solution using an acid ion-exchange resin. Before ion exchanging the zeolites that contained organic amine cations they were calcined in an $NH_3$ atmosphere to decompose the organic cation and then exchanged with a sodium salt solution. The resulting products had the same SAR as the uncalcined zeolites and an Na/Al ratio of 1.

These sodium zeolites were then ion exchanged by contacting them with Dowex 50W-X8 in the $H_3O^+$ form that was separated from the zeolite by a dialysis membrane. The $H_3O^+$-$Na^+$ ion exchange occurred in infinitely dilute solution eliminating acid attack of the zeolites. In some cases exchange was done with dilute acid for comparision. Their ion-exchange isotherms are shown in Figs. 57–61.

All of the zeolites maintained SAR, exchangeable-cation/aluminum ratio, and crystallinity after $H_3O^+$ ion exchange as well as after back-exchange with $Na^+$. Figures 57 and 58 show cut-offs of 80% and 66% exchange for zeolites Y and ZSM-4 using Dowex 50W-X8 in the $H_3O^+$ form. Figures 59 and 61 show that exchange of NaZSM-5 and mordenite with $H_3O^+$ ions using the hydrogen resin and using 0.1 N HCl give the same results. No crystallinity is lost when 0.1 N HCl was used. The zeolite could be completely re-exchanged with $Na^+$ ions in both cases.

All of the high-silica zeolites show a high selectivity for $H_3O^+$ ions over $Na^+$. However, only 72% of the $Na^+$ ions could be replaced from NaY and only 67% could be replaced from NaZSM-4. In the case of zeolite Y the remaining $Na^+$ ions are probably in the sodalite cages and hexagonal prisms. In the case of ZSM-4 the remaining $Na^+$ are probably in the gmelinite cages of this structure (40).

Copyright © 2003 Marcel Dekker, Inc.

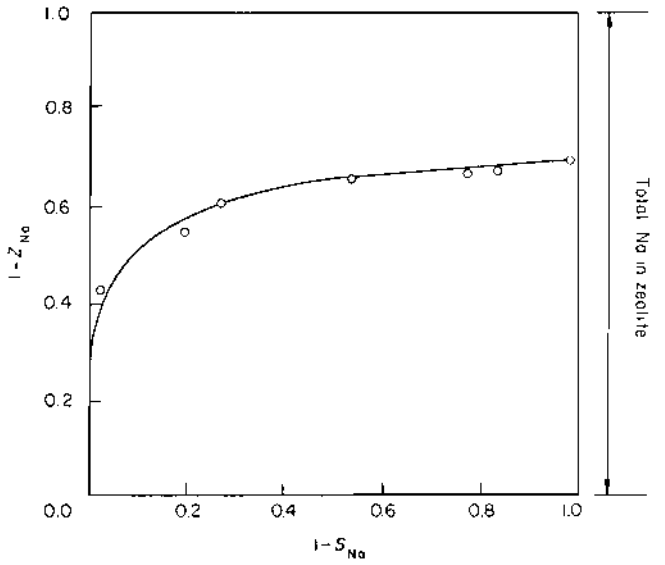


**Fig. 58** $H_3O^+$-$Na^+$ exchange isotherm of ZSM-4 using Dowex 50X8 at 25°C. (From Ref. 39.)

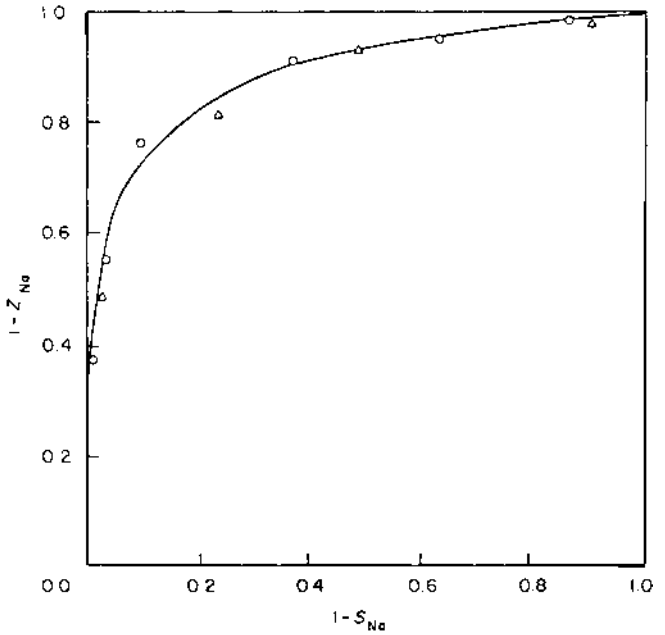


**Fig. 59** $H_3O^+$-$Na^+$ exchange isotherm of precalcined ZSM-5 at 25°C; ○, 0.1N HCl; Δ Dowex 50X8. (From Ref. 39.)

Copyright © 2003 Marcel Dekker, Inc.

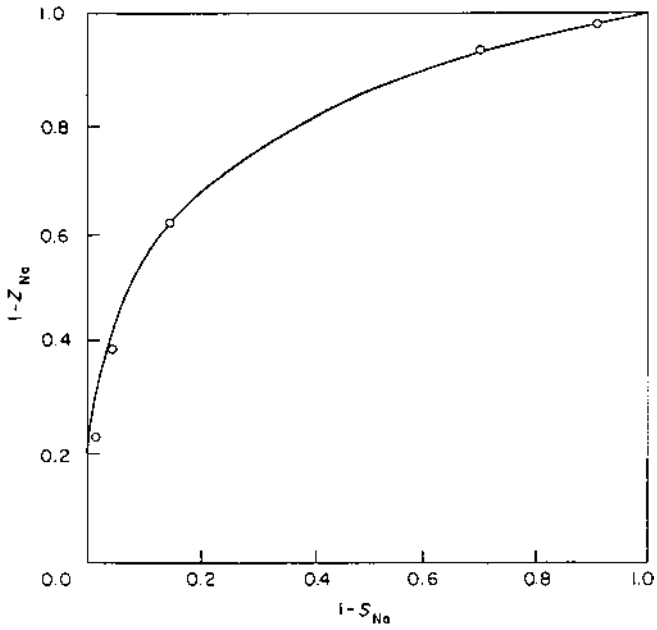


**Fig. 60** $H_3O^+$-$Na^+$ exchange isotherm of ZSM-11 using Dowex 50X8 at 25°C. (From Ref. 39.)

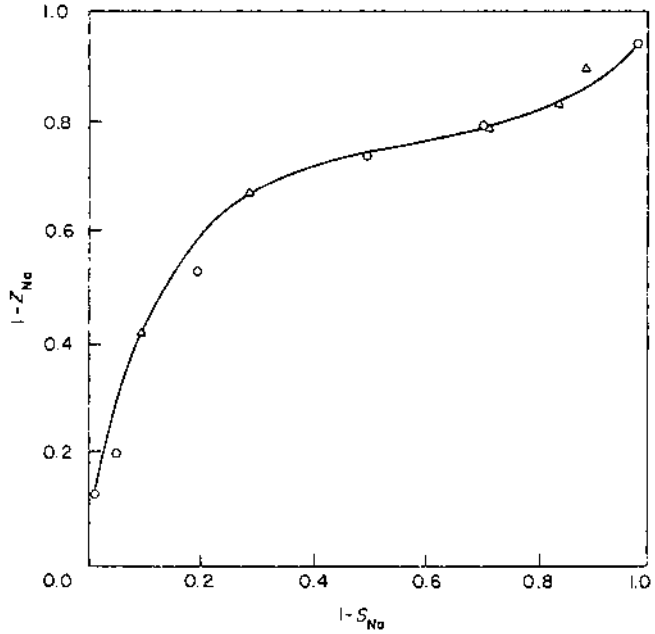


**Fig. 61** $H_3O^+$-$Na^+$ exchange isotherm of mordenite at 25°C; ○, 0.1N HCl; Δ Dowex 50X8. (From Ref. 39.)

Copyright © 2003 Marcel Dekker, Inc.

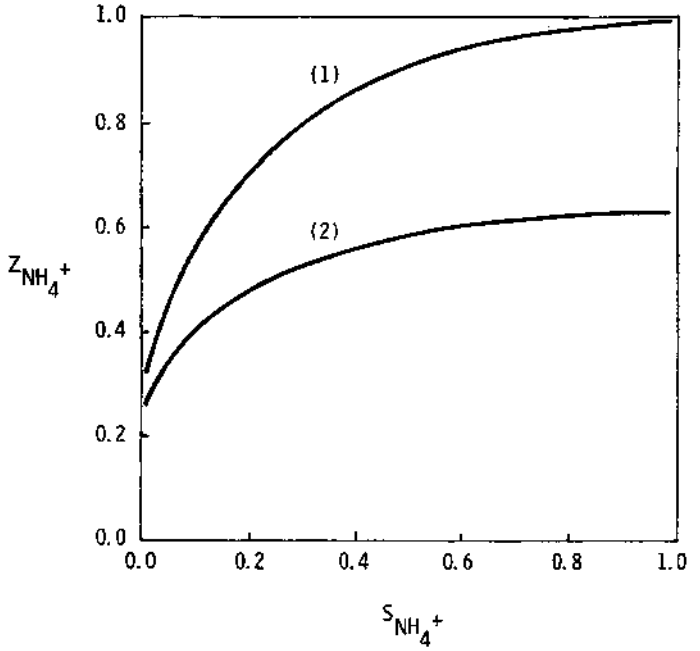


**Fig. 62** The $NH_4^+$–$Na^+$ exchange isotherms of ZSM-5 at 25°C. (1) Pure Na form, organics removed. (2) As synthesized. (From Ref. 41.)

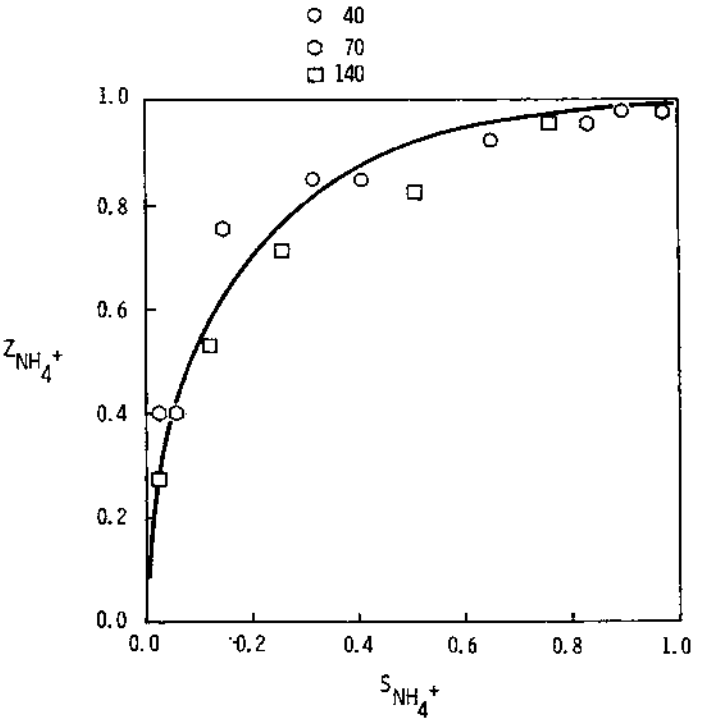


**Fig. 63** The $NH_4^+$–$Na^+$ exchange isotherms of ZSM-5 of varying SAR at 25°C. ○, 40; ⬭, 70; □, 140. (From Ref. 41.)

Copyright © 2003 Marcel Dekker, Inc.

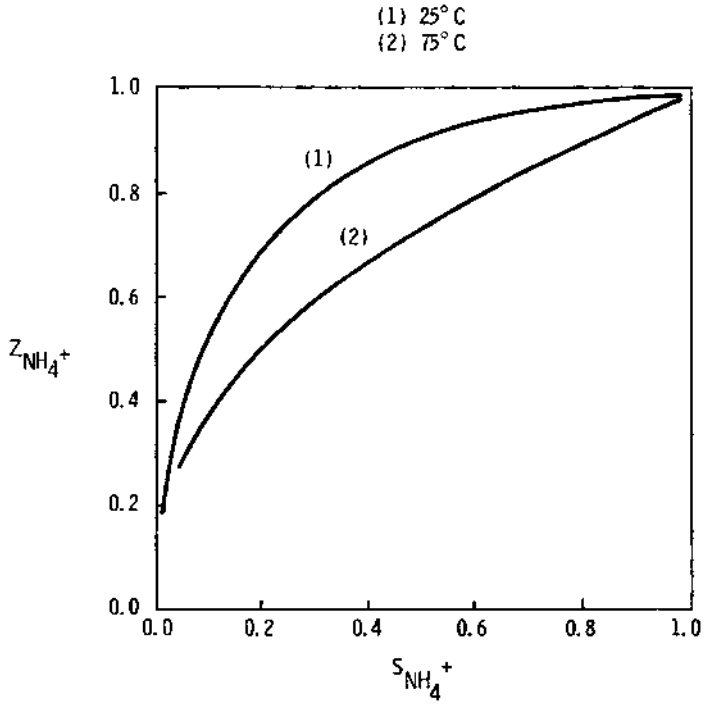


**Fig. 64** The dependence of ZSM-5 selectivity on the temperature of equilibration of $NH_4^+$–$Na^+$ exchange isotherms: (1), 25°C; (2) 75°C. (From Ref. 41.)

## B. Inorganic Ion Exchange of ZSM-5

A valuable study of the ion-exchange properties of ZSM-5 was done by Chu and Dwyer (41) in 1983. They prepared the $NH_4^+$ and $Na^+$ forms of ZSM-5 with SARs of 40 and 70 and ZSM-11 with a SAR of 77.5 by calcination of the as-synthesized zeolites in an ammonium atmosphere followed by exhaustive $NH_4^+$ or $Na^+$ ion exchange. Their ion-exchange isotherms are shown in Figs. 62–69. Figure 62 shows that if one attempts to exchange ammonium ion into the as-synthesized TPA-ZSM-5 only partial exchange is possible. Occluded salts and possible trapping of TPA cations are responsible. On the other hand, the isotherm for the pure Na form shows complete exchange. Figures 63 and 64 show the high selectivity of the zeolite for $NH_4^+$ ions over $Na^+$ ions. They also show that the selectivity for $NH_4^+$ varies little with SAR and decreases with increasing temperature. The isotherms in Figs. 65 and 66 involve ion exchange of the $NH_4^+$ form of ZSM-5. Examination of these isotherms shows that $Cs^+$ and $H_3O^+$ ions are preferred to ammonium ions and can replace all of the cations in the zeolite. All of the other alkali metal cations are preferred much less than ammonium ion. The selectivity series for univalent ions is $Cs > H_3O > NH_4 > K > Na > Li$. This series is in the decreasing order of the size of the bare ions. The isotherms for $Cu^{2+}$ and $Zn^{2+}$ show a slight preference over $Na^+$ ions whereas the one for $Ni^{2+}$ shows a slight preference for $Na^+$ (Figs. 67–69). More importantly, the isotherms involving divalent transition metal ion exchange show that all of the $Na^+$ ions are replaced.

In a later work, Mathews and Rees (42) and McAleer et al. (43) also studied inorganic ion exchange in ZSM-5 as a function of SAR. They prepared Na-ZSM-5 by

Copyright © 2003 Marcel Dekker, Inc.

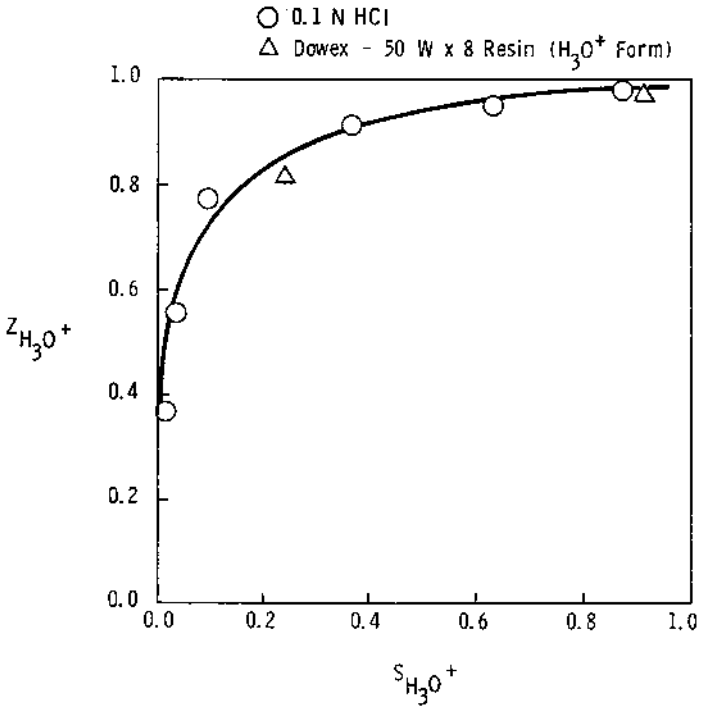


**Fig. 65** Ion-exchange isotherms of $H_3O^+$ ions with $NH_4$ZSM-5 at 25°C. ○, 0.1 N HCl; Δ, Dowex 50X8. (From Ref. 41.)

calcining the as-synthesized TPA-ZSM-5 in air and then exhaustively ion-exchanging the zeolite with $Na^+$ ions. This procedure is to be compared to the calcination in an ammonia atmosphere used by Chu and Dwyer (39,41), which probably introduced fewer faults into the zeolite structure. Nevertheless, calcination in air as done by Rees and coworkers is the most widely used procedure to prepare ZSM-5 catalysts.

Matthews and Rees (42) found that all of the $Na^+$ ions in Na-ZSM-5 were replaced by the other alkai metal cations regardless of SAR (they expressed SAR in terms of the number of Al atoms per unit cell, S = Al). Even the large $Cs^+$ ion replaced all of the $Na^+$ ions. Chu and Dwyer (41) already had reported that $Cs^+$ ions replaced all of the ammonium ions in $NH_4$-ZSM-5. McAleer et al. (43) found that $K^+$ ions can replace all of the $Na^+$ ions in Na-ZSM-5 regardless of the SAR (Fig. 70), but the degree of exchange with alkaline earth cations depends on the SAR of the zeolite and the ionic radii of the bare ions (Fig. 71). They showed that the maximal degree of divalent ion exchange increases with decreasing SAR and increases with increasing bare ion size. These results are more easily seen in Fig. 72.

Why does a large cesium ion replace all of the sodium ions in Na-ZSM-5 regardless of SAR while the much smaller alkaline earth ions cannot? McAleer et al. (43) used a Monte Carlo simulation of the Al-Al distances in the zeolite structure to explain these results. This simulation showed that there is a distribution of Al-Al distances that varies with SAR. Their calculations showed that the distribution of Al-Al distances shifts to lower values with decreasing SAR. From these calculations and the experimentally determined maximal degrees of ion exchange, they concluded that the larger the bare divalent ion the larger the Al-Al distance that could be covered. If

Copyright © 2003 Marcel Dekker, Inc.

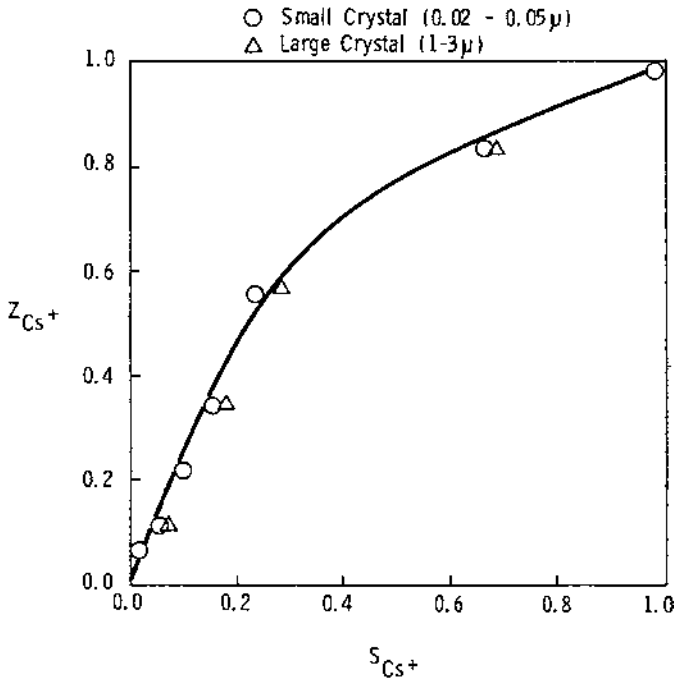


**Fig. 66** Effect of crystal size on the $Cs^+$-$NH_4^+$ ion exchange isotherm of ZSM-5 at 25°C: ○, small crystal (0.02–0.15 μm); Δ, large crystal (1–3 μm). (From Ref. 41.)

the bare divalent ion can cover two Al sites it can replace the two $Na^+$ ions that are associated with those sites. A much simpler electrostatic argument was used by Sherry (44) in 1969 to show the difficulty in exchanging $Na^+$ ions from zeolites as a function of SAR. This approach allows calculation of the standard free energy of exchange of univalent ions by divalent but does not allow for a distribution of Al-Al distances. It assumes an average Al-Al distance.

### C. Organic Ion Exchange of ZSM-5

In 1988, Chu and Dwyer (45) described their work on organic ion exchange of Na-ZSM-5. They prepared the Na form of ZSM-5 with SARs of 40 and 70 and ZSM-11 with a SAR of 77.5 using the technique described above. They then studied ion exchange of Na-ZSM-5 with tetramethylammoniuim ion (TMA), tetraethylammonium ion (TEA), tetrapropylammonium (TPA), benzyltrimethylammonium (BTMA), and $C_1$–$C_4$ mono-*n*-alkylammonium and di-*n*-alkylammonium (MA, EA, PA, BA, $M_2A$, $E_2A$, $P_2A$, $B_2A$) ions. Na-ZSM-5 shows high selectivity for all of these organic cations. Of course, the organic cations that are too large to fit into the small pores of the zeolite structure cannot replace all of the $Na^+$. The authors show that the selectivity sequence correlates with ionic size:

$$Na << MA < EA < PA < BA$$

$$Na << M_2A > E_2A < P_2A < B_2A$$

$$MA < M_2AL < TMA$$

Copyright © 2003 Marcel Dekker, Inc.

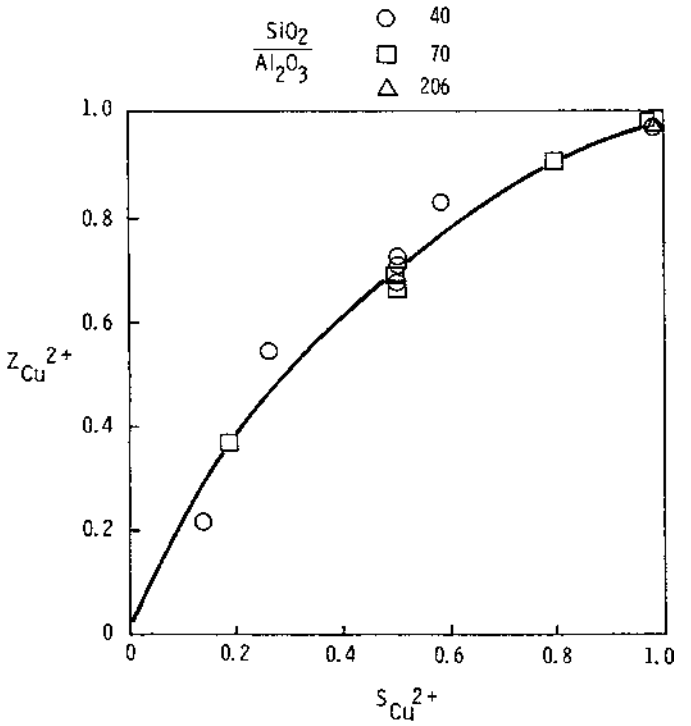


**Fig. 67** $Cu^{2+}$-$Na^{+}$ ion-exchange isotherm of ZSM-5 at 25°C. $SiO_2/Al_2O_3$ = 40 (○), 70 (□), 206 (Δ). (From Ref. 41.)

The ion-exchange isotherms that are shown in Fig. 73 indicate that MA, $M_2A$, EA, PA, and BA cations can replace all of the $Na^{+}$ ions in ZSM-5 and also demonstrates the selectivity sequence shown above. The isotherms in Fig. 74 show that complete exchange is possible with TMA ion and not with BTMA ions. BTMA are too large to fit into the sinusoidal channels of ZSM-5 and cannot replace 35% of the $Na^{+}$. It is reasonable to conclude that 35% of the $Na^{+}$ ions reside in the small elliptical channels and 65% reside in the large straight channels of the zeolite. Figure 75 shows that complete exchange of Na-ZSM-11 is possible with BTMA ions whereas only 65% exchange is possible in ZSM-5. ZSM-11 only has straight channels of the same size as those in ZSM-5 (46).

## D. Ion Exchange in EU-1

Watlings and Rees studied ion exchange in EU-1 (47,48). The zeolites were prepared for ion exchange by calcining in air to remove the organic templates used in their synthesis followed by exhaustive exchange with $Na^{+}$ ions. The selectivity for the univalent ions used was $Na < K < H_3O < Cs$. This sequence is also the sequence of the size of the bare ion. Complete replacement of $Na^{+}$ was accomplished by $K^{+}$, $Cs^{+}$, and $H_3O^{+}$ ions and the reactions were reversible.

On the other hand, complete exchange could not be accomplished with $Ca^{2+}$, $Sr^{2+}$, and $Ba^{2+}$ ions and the maximal degree of exchange increased with decreasing SAR and

Copyright © 2003 Marcel Dekker, Inc.

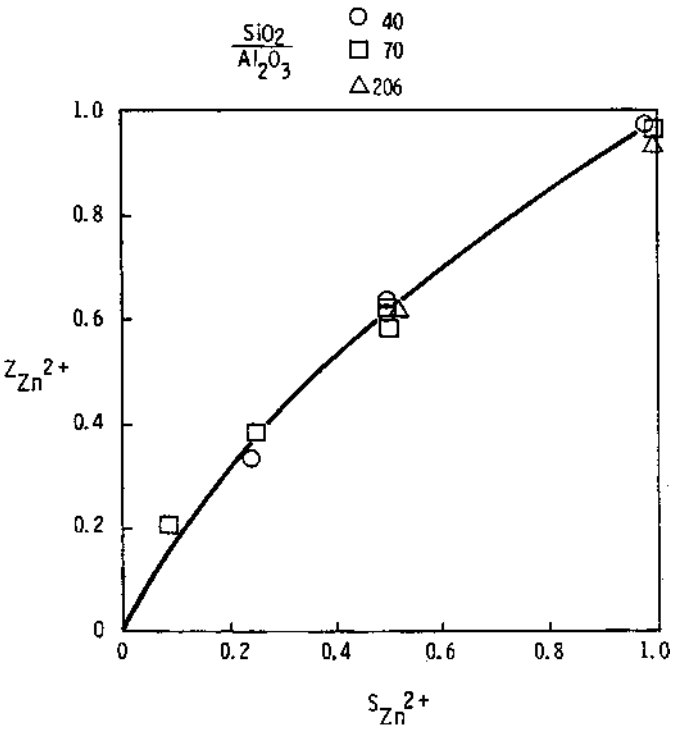


**Fig. 68** $Zn^{2+}$-$Na^{+}$ ion-exchange isotherm of ZSM-5 at 25°C. $SiO_2/Al_2O_3$ = 40 (○), 70 (□), 206 (Δ). (From Ref. 41.)

increasing bare ion size. These results are similar to those obtained with ZSM-5 (42) and were explained using the same kind of Monte Carlo simulation (43).

## VIII. GENERALIZATIONS OR THE RULES OF ION EXCHANGE

Based on the ion-exchange studies that have been reviewed, the following generalizations can be made:

1. All zeolites prefer $Na^{+}$ to $Li^{+}$.
2. All zeolites prefer $NH_4^{+}$ to $Na^{+}$.
3. The most aluminous zeolites have the highest selectivity for $Ca^{2+}$ and other alkaline earth cations and this selectivity decreases with increasing SAR. This trend should be even more marked for trivalent cations.
4. The most siliceous zeolites have the highest selectivity for $Cs^{+}$, $Rb^{+}$, $NH_4^{+}$, and $K^{+}$. This selectivity decreases with decreasing SAR.
5. Selectivity will increase with decreasing salt concentration if the ingoing cation has a higher charge than the outgoing cation. Selectivity will decrease with increasing salt concentration.
6. In zeolites with very high SAR, complete ion exchange of divalent ions for monovalent ions becomes very difficult. Selectivity and degree of exchange increases with increasing size of the divalent ion and decreasing SAR. Trivalent

Copyright © 2003 Marcel Dekker, Inc.

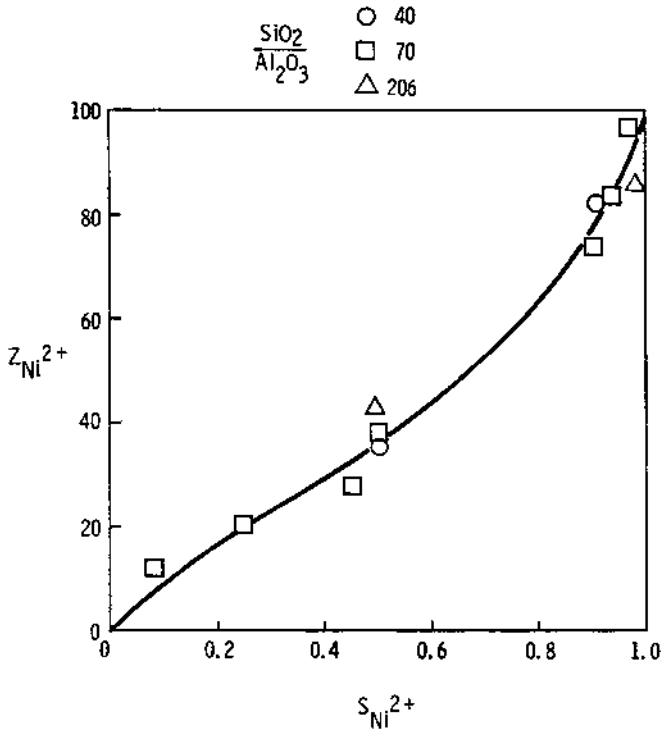


**Fig. 69** $Ni^{2+}$-$Na^{+}$ ion-exchange isotherm of ZSM-5 at 25°C. $SiO_2/Al_2O_3$ = 40 (○), 70 (□), 206 (Δ). (From Ref. 41.)

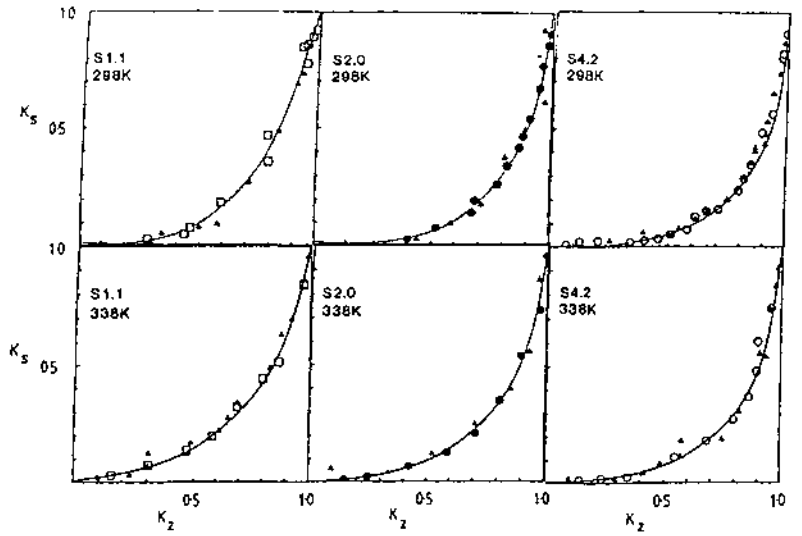


**Fig. 70** Na/K isotherms at 298 K and 338 K in ZSM-5 with 1.1, 2.0, and 4.2 Al per unit cell. (▲) Reverse isotherms. (From Ref. 43.)

Copyright © 2003 Marcel Dekker, Inc.

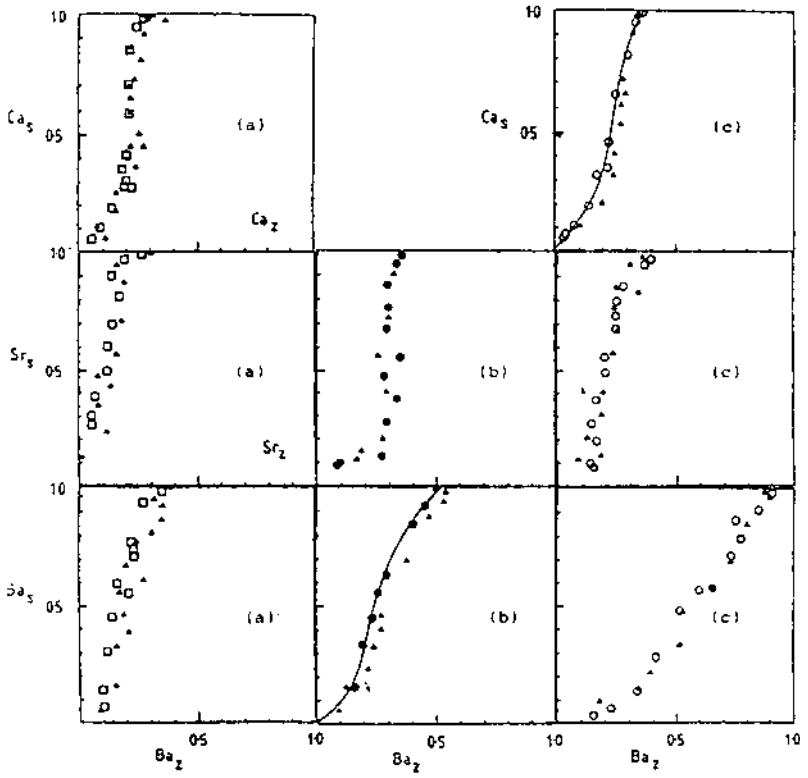


**Fig. 71** Na-divalent cation exchange at 298 K in ZSM-5 with (a) 1.1, (b) 2.0, and (c) 4.2 A1 per unit cell. (▲) Reverse isotherms. (From Ref. 43.)

cations should be even more difficult to exchange into zeolites with very high SAR.

7. All zeolites are highly selective for polarizable ions such as $Ag^{+}$, $Tl^{+}$, $Pb^{2+}$, and $Cd^{2+}$. However, the lower the SAR the higher the selectivity.
8. Partial ion exchange may take place where ions are located in large and small cages and the ingoing hydrated ion or bare ion is too large to diffuse into the small cages.
9. Redistribution of the cations that are initially present in a zeolite may take place if the ingoing cation is very large. Therefore, incomplete exchange is not necessarily an indication of ion sieving. It may be a result of ion crowding.
10. Zeolites with a SAR of 10 or higher can undergo reversible hydronium ion exchange using strong acids.

## IX. THERMODYNAMICS OF ION EXCHANGE

The phase distribution data that we obtain in the form of ion-exchange isotherms can be used to calculate standard free energies, enthalpies, and entropies of ion exchange. In the case of incomplete exchange, or ion sieving, the ordinates are normalized so that 100%

Copyright © 2003 Marcel Dekker, Inc.

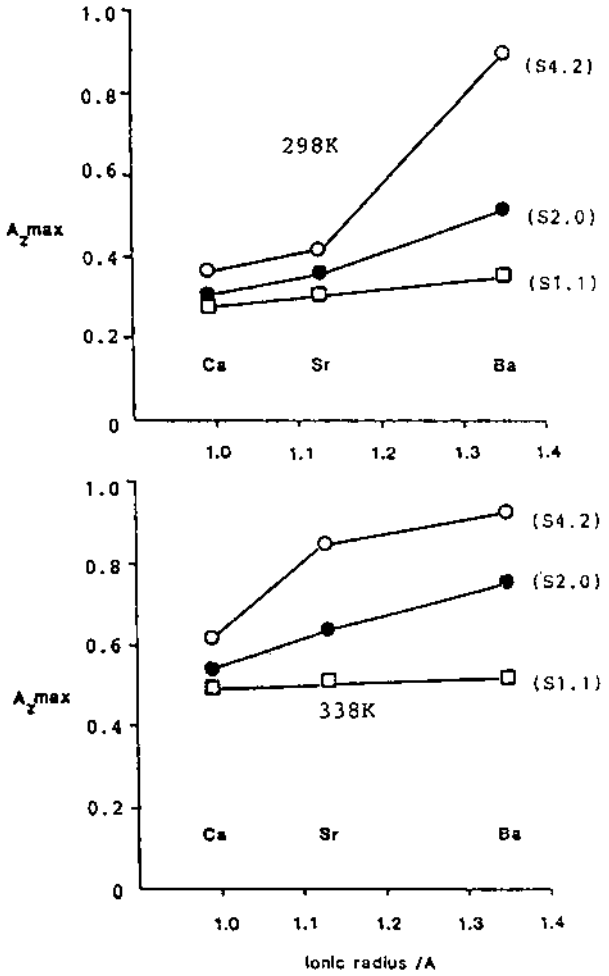


**Fig. 72** Maximal exchange level in ZSM-5 for divalent cations at 298 and 338 K as a function of cation radius. (From Ref. 43.)

exchange represents replacement all of the exchangeable ions. In order to calculate the standard free energy, the rational selectivity coefficient for the reaction

$$b\mathrm{A}_s^{a+} + a\mathrm{B}_z^{b+} \rightleftharpoons b\mathrm{A}_z^{a+} + a\mathrm{B}_s^{b+} \tag{6}$$

is defined by the equation:

$$K = \frac{f_A{}^b Z_A{}^b \gamma_B{}^a m_B{}^a}{f_B{}^a Z_B{}^a \gamma_A{}^b m_A{}^b} = \frac{{}^N K_B f_A{}^b{}_B{}^a}{f_B{}^a \gamma_A{}^b} \tag{7}$$

where $f_A$ and $f_B$ are the rational single ion activity coefficients of ions A and B in the zeolite phase, $\gamma_A$ and $\gamma_B$ are the molal acitivity coefficients of ions A and B in the solution phase, $Z_A$ and $Z_B$ are the equivalent fractions of ions A and B in the zeolite phase, $m_A$ and

Copyright © 2003 Marcel Dekker, Inc.

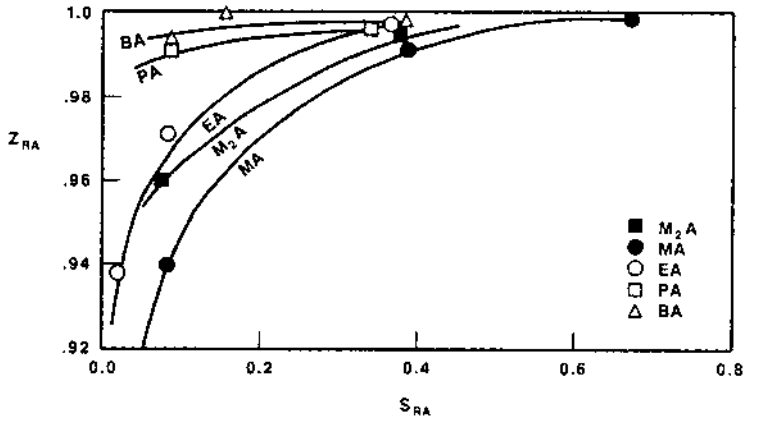


**Fig. 73** Alkylammonium ion exchange in ZSM-5 at 25°C. High-exchange portion; SAR = 70. (From Ref. 45.)

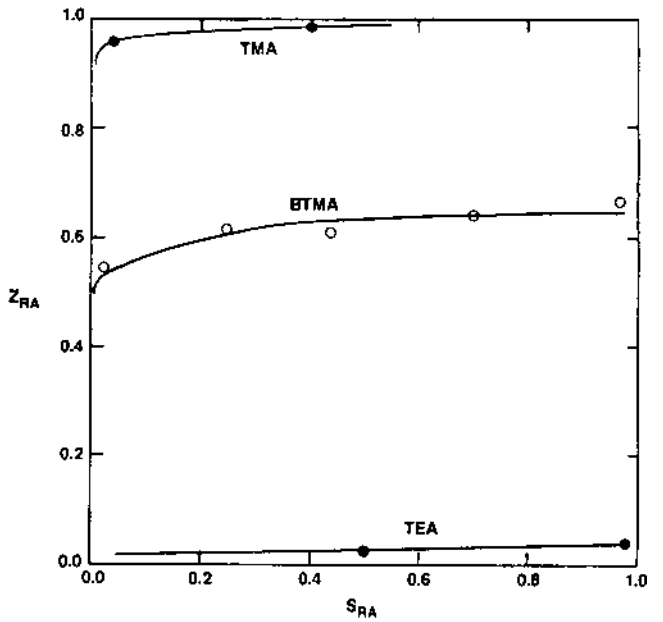


**Fig. 74** Pore systems of ZSM-5 illustrated by its TMA, BTMA and TEA ion-exchange isotherms; SAR = 70. (From Ref. 45.)

Copyright © 2003 Marcel Dekker, Inc.

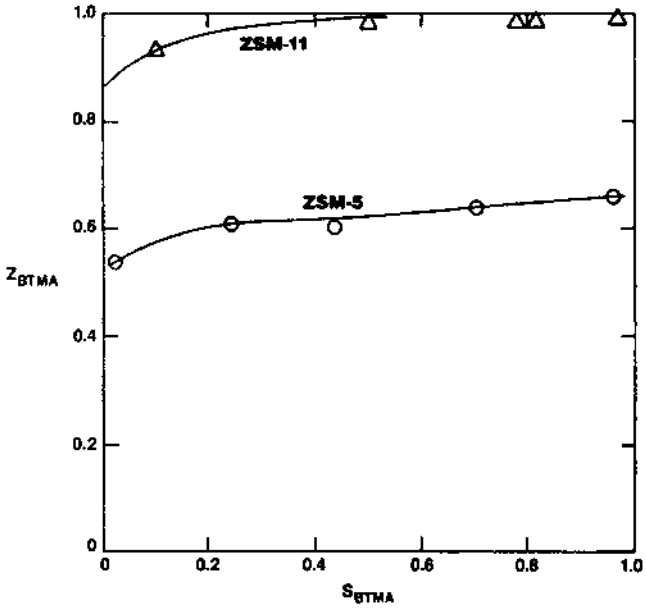


**Fig. 75** BTMA-Na exchange isotherm of ZSM-5 and ZSM-11 at 25°C; ZSM-5 (SAR = 70); ZSM-11 (SAR = 80). (From Ref. 45.)

$m_B$ are the molalities of ions A and B in the solution phase, $K$ is the thermodynamic equilibrium constant for the ion exchange reaction, s and z are the subscripts that identify the solution and zeolite phases, and ${}^{N}K_B$ is the rational selectivity coefficient or the concentration quotient.

The corrected rational selectivity coefficient $K_c$ is defined as:

$$K_{cB}{}^{A} = \frac{{}^{N}K_B{}^{A}\gamma_B{}^{a}}{\gamma_A{}^{b}} = \frac{Kf_B{}^{a}}{f_A{}^{b}} \tag{8}$$

$$K_{cB}{}^{A} = {}^{N}K_B{}^{A}\frac{[\gamma_{\pm BYb}{}^{b+1}]^{a}}{[\gamma_{\pm AYa}{}^{a+1}]^{b}} \tag{9}$$

where $\gamma_{\pm BYb}$ and $\gamma_{\pm AYa}$ are the mean molal activity coefficients for the salts $BY_b$ and $AY_a$. Equation (8) states that any variation in the corrected rational selectivity coefficient is due to variation in the single ion activity coefficients in the zeolite phase. Equation (9) states that the corrected rational selectivity coefficient can be calculated from knowledge of the concentration quotient and the mean molal activity coefficients.

The method of Gaines and Thomas (1) can be used to calculate the natural logarithm of the equilibrium constant, ln $K$. A modified version of their equation that assumes that the mean molal activities are 1 in dilute solution is:

$$\ln K = (b - a) + \int_0^1 \ln K_C \, dZ_A \tag{10}$$

The first term on the right hand side of Eq. (10) is the difference between the charge on the exchanging ions. The integral in Eq. (10) is graphically evaluated by plotting the log $K_{cB}{}^{A}$

Copyright © 2003 Marcel Dekker, Inc.

vs $Z_A$ and graphically integrating the area under the curve that is obtained. If data are obtained at three or more temperatures, the standard free energy, standard enthalpy, and standard entropy of exchange can be calculated from the relationships:

$$\Delta F_T^\circ = -RT \ln K \tag{11}$$

$$\frac{d \ln K}{dT} = \frac{\Delta H^\circ}{RT^2} \tag{12}$$

$$\Delta S^\circ = \frac{\Delta H^\circ - \Delta F_T^\circ}{T} \tag{13}$$

where $R$ is the ideal gas constant and $T$ is the absolute temperature.

In a thermodynamic analysis of alkaline earth ion exchange of NaX and NaY done by Sherry in 1966 (7), the standard enthalpies of exchange for $Ca^{2+}$ and $Sr^{2+}$ were shown to be positive. The standard free energies of exchange were negative because of a large increase in entropy as a result of ion exchange. This is shown in Table 1. In the case of $Ba^{2+}$ ion exchange of the $Na^+$ in the large cages of zeolites NaX and NaY, the standard free energy of the reaction is a large negative number because the standard enthalpy is also negative. These data show that these ion-exchange reactions are entropy directed.

Using entropies and enthalpies of hydration for $Ca^{2+}$ and $Sr^{2+}$ taken from Ref. 16, Sherry calculated (7) the changes in enthalpy and entropy that occur in the zeolite and solution phases as a result of the exchange reactions. The results of these calculations are shown in Table 2. The data in the table show that for $Ca^{2+}$ and $Sr^{2+}$ ion exchange of NaX and NaY most of the increase in entropy occurs in the aqueous phase. Similar results were obtained $Ca^{2+}$ and $Sr^{2+}$ of NaA (27). These reactions are also entropy controlled. This thermodynamic analysis leads to the conclusion that in zeolites NaA, NaX, and NaY ion exchange selectivity is determined by the solution phase. Clearly the aqueous phase prefers $Na^+$ ions to the $Ca^{2+}$ and $Sr^{2+}$ ions because entropy of the solution is greater when it contains $Na^+$ ions than when it contains $Ca^{2+}$ or $Sr^{2+}$ ions. It is likely the case for other zeolites with open frameworks.

**Table 1** Standard Free Energies, Enthalpies, and Entropies of Reaction

| | $\Delta G^\circ_T$, cal/equiv | | | | |
|---|---|---|---|---|---|
| Reaction | 278 K | 298 K | 323 K | $\Delta H^\circ$, cal/eq | $\Delta S^\circ$, eu/eq |
| $Ca^{2+}$ + 2NaX | | −320 ± 10 | −460 ± 20 | 1200 ± 100 | 5.1 ± 0.5 |
| $Ca^{2+}$ + 2NaY | | −420 ± 10 | −470 ± 20 | 640 ± 50 | 3.6 ± 0.4 |
| $Sr^{2+}$ + 2NaX | | −740 ± 20 | −850 ± 30 | 530 ± 50 | 4.3 ± 0.4 |
| $Sr^{2+}$ + 2NaY | −370 ± 15 | −510 ± 20 | −680 ± 20 | 1540 ± 150 | 6.9 ± 0.7 |
| $Ba^{2+}$ + 2NaX | −1250[a] ± 30 | −1310[a] ± 30 | −940[b] ± 30 | −430[a] ± 80 | 3.0 ± 0.6 |
| | | | −1080[c] ± 30 | | |
| $Ba^{2+}$ + 2NaY | | −870 ± 20 | −840 ± 20 | −350 ± 30 | 1.8 ± 0.2 |

[a] Refers to complete exchange of the large cages and no replacement of $Na^+$ ions in the small cages.
[b] Refers to complete exchange of all the $Na^+$ ions in all the cavities.
[c] The free energy for the replacement of only the $Na^+$ ions in the small cages.

Copyright © 2003 Marcel Dekker, Inc.

**Table 2** Entropy and Enthalpy Changes in Aqueous and Zeolite Phases

| $M^{2+}$ | $1/2\,S_M^{2+\,hyd} - S_{Na}^{hyd\,a}$ eu/equiv of zeolite | $1/2\,S_M^{2+\,zeol} - S_{Na}^{zeol}$, eu/equiv of zeolite | $1/2\,H_M^{2+\,hyd} - H_{Na}^{hyd\,a}$, cal/equiv of zeolite | $1/2\,H_M^{2+\,zeol} - H_{Na}^{zeol}$, cal/equiv of zeolite |
|---|---|---|---|---|
| CaX | −4.2 | 1.0 | −93,400 | −92,200 |
| CaY | −4.2 | −0.6 | −93,400 | −92,800 |
| SrX | −3.4 | 0.9 | −75,700 | −75,000 |
| SrY | −3.4 | 3.6 | −75,700 | −75,200 |
| BaX | 1.95 | 4.65 | −58,700 | −59,130 |
| BaY | 1.95 | 3.65 | −58,700 | −59,050 |

[a] Values calculated from data in Ref. 7.

## X. SALT IMBIBEMENT

Salt imbibement in zeolites is a phenomenon that has been seldom reported in the literature, is often ignored, and is often encountered in both laboratory and commercial ion-exchange operations. Electrolyte imbibement has been studied in gel ion exchangers, and the results are reasonably well explained by the Donnan membrane equilibrium (49). Imbibement can be explained in the following way: The concentration of $Na^+$ ions in the large cavities of NaA is extremely high, much higher than can be achieved in an aqueous solution of NaCl. When NaA is immersed in an NaCl solution there is a thermodynamic driving force for $Na^+$ ions to diffuse into the aqueous solution because of the concentration gradient between the zeolite and solution phases. There is also a thermodynamic driving force arising from differences in the concentration of $Cl^-$ in the zeolite and solution. The diffusion of cations ($Na^+$) into the solution and anions ($Cl^-$) into the zeolite results in the accumulation of negative charge in the zeolite and positive charge in the solution. The first few ions that diffuse cause an electric potential difference to build up between the two phases. This potential, called the Donnan potential, pulls cations back into the zeolite and anions back into the solution. Equilibrium is reached in which the tendency of the ions to level out concentration differences is balanced by the action of the electric field. This equilibrium is called the Donnan membrane equilibrium. It has been well characterized for gel-type exchangers. If the external salt concentration is very high, anions can diffuse into the zeolite and carry along cations to preserve electrical neutrality in both phases.

Platek and Marinsky (50) and Barrer and Meier (51) showed that salt molecules may occur in the zeolitic water in the crystals. Barrer and Walker (52) studied salt uptake, or imbibement, of alkali metal halides by alkali metal forms of zeolites X, Y, and A. Their work clearly shows that, at low concentration of salt in the aqueous phase, salt is excluded from the zeolite. Thus, below 0.5 N salt concentration, imbibement is negligable. The Donnan potential maintains a concentration gradient between the interior of the zeolite and the salt solution. At high salt concentration in the solution the concentration gradient overwhelms the Donnan potential and salt imbibement takes place. It increases with increasing salt concentration. Some salt uptake curves from Barrer and Walker (52) are shown in Fig. 76.

Barrer and Walker (52) also demonstrated that equilibrium salt uptake is independent of the anions with the same charge but did demonstrate that salt exclusion is greater if the anion is divalent. They also showed that uptake of halides by NaA is

Copyright © 2003 Marcel Dekker, Inc.

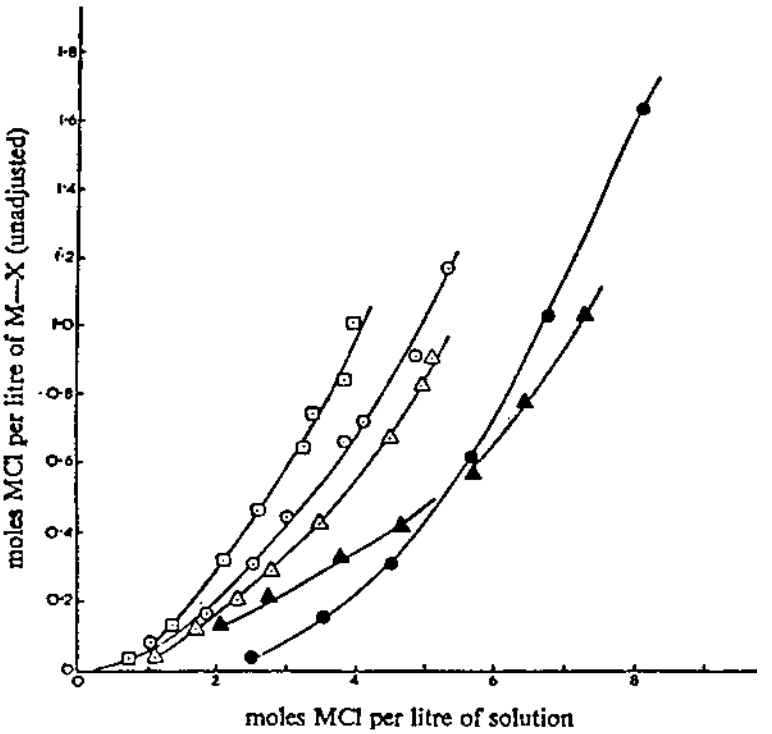


**Fig. 76** The influence of the cation upon salt inclusion as shown by the 25°C isotherms of various chlorides in zeolite X □, KC1; ○, NaCL; ●, $CaCl_2$; △, LiCl; ▲, CsCl (From Ref. 52.)

extremely slow. In fact, at 25°C there is no measurable uptake of NaCl. It took a few days to reach equilibrium at 90°C. The slow diffusion of anions into this zeolite is a size effect. The free diameter of the eight-ring window into zeolite A is 4.0 Å as compared with 3.62, 3.92, 4.32, and 5.5 Å for $Cl^-$, $Br^-$, $I^-$, and $SO_4^{2-}$. Obviously, the Donnan membrane equilibrium will be violated if the anion is excluded based on size. The foregoing explanation of the origin of the Donnan potential suggests that salt imbibement will be greater in zeolites with a high SAR.

Most commercial ion-exchange processes used to modify zeolites use concentrated salt solutions to minimize tank size. Washing of occluded salts is often a difficult problem. Washing should be done at the same temperature and for the same time as ion exchange. Often higher temperatures and longer contact times are required to wash the zeolite free of occluded salt.

## XI. DESIGN OF ION EXCHANGE PROCESSES

### A. General Approach

Sherry (2) has developed and described a graphical technique for designing ion-exchange processes that only requires knowledge of the ion-exchange isotherm. This graphical technique will be summarized in this section for two of the most common ion-exchange processes. One is the crossflow method in which a batch of zeolite is contacted consecutively with fresh portions of the exchange solution until the desired degree of exchange is

Copyright © 2003 Marcel Dekker, Inc.

attained. The other method is a countercurrent process in which the zeolite and the solution move countercurrent to each other in a stagewise manner. Crossflow operation is the process most used in preparing laboratory samples.

## B. Assumptions and Nomenclature

The assumptions that are made in the mathematical and graphical treatment that follows are listed below:

- The water content of the hydrated zeolite does not change as a result of ion exchange.
- The process occurs at constant normality and temperature.
- Each stage of the process is isothermal.
- Continuous countercurrent operations are at steady state.
- Equilibrium is reached in each stage.
- Salt imbibement is negligible.
- Perfect phase separation occurs in each stage.

Salt imbibement is negligible below 0.5 total normality of salt. Most laboratory operations are done in dilute solution. It is the reason that all of the isotherms obtained in a pure research situation are obtained at 0.1 N. Perfect phase separation is also obtainable in a laboratory situation. Although the last two assumptions are not very valid in a plant process, the graphical technique does give a good approximation of the data.

The nomenclature used in what follows is shown in Table 3.

## C. Crossflow Operation

The flow diagram for the crossflow process is shown in Fig. 77. Consider the exchange of $K^+$ ion into NaX. The reaction is

$$K^+ + NaX \rightleftharpoons Na^+ + KX \tag{14}$$

A material balance for $K^+$ about the $m$th stage results in the following equation:

$$Z_{m-1} W_{m-1} u_{m-1} + S_o N_{To} v_o = Z_m W_m u_m + S_m N_{Tm} v_m \tag{15}$$

**Table 3** Nomenclature

| | |
|---|---|
| $C$ | a constant = $N_T v$ = the number of equivalents of salt in solution fed into a stage in a batch process. |
| $C'$ | a constant = $N_T v'$ = the number of equivalents of salt in solution flowing per unit time in a continuous process. |
| $m$ | $m$th stage in a multistage process. |
| $n$ | last stage in a multistage process. |
| $N_T$ | total normality. |
| $Q$ | constant = $Wu$ = the number of equivalents of zeolite fed to a stage in a batch process. |
| $Q'$ | a constant = $Wu'$ = the equivalents of zeolite flowing per unit time in a continuous process. |
| $S$ | equivalent fraction in solution of the ion for which a material balance is being made. |
| $u$ | grams of dry zeolite entering a stage in a batch process. |
| $u'$ | grams of dry zeolite flowing per unit time in a continuous process. |
| $v$ | liters of solution entering a stage in a batch process. |
| $v'$ | liters of solution flowing per unit time in a continuous process. |

Copyright © 2003 Marcel Dekker, Inc.

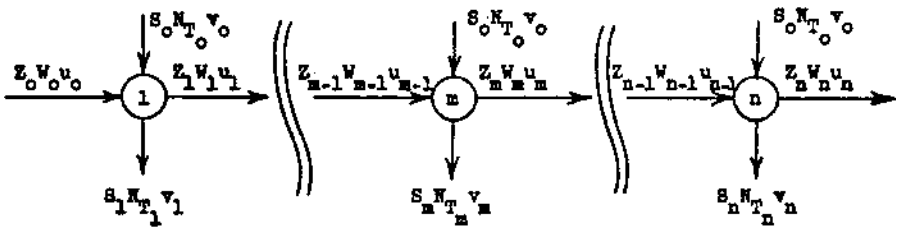

**Fig. 77** Flow diagram for crossflow operation. (From Ref. 2.)

The mass of zeolite and the volume of solution change as a result of ion exchange. However, the products ($Wu$) and ($N_T V$), the total equivalents in the mass of zeolite and in the volume of solution, are constant throughout the exchange process. Therefore,

$$W_m U_m = W_{m-1} u_{m-1} = Q = \text{constant} \tag{16a}$$

$$N_{Tm} v_m = N_{To} v_o = C = \text{constant} \tag{16b}$$

Solution of Eqs. (15) and (16) results in

$$\frac{Z_m - Z_{m-1}}{S_m - S_o} = \frac{-C}{Q} \tag{17}$$

Equation (17) describes a straight line with a slope of $-C/Q$ that passes through the points ($S_m$, $Z_m$) and ($S_o$, $Z_{m-1}$). The point ($S_m$, $Z_m$) represents the concentrations of the stream leaving the $m$th stage and is also a point on the equilibrium ion-exchange isotherm. It is important to realize that the material balance Eq. (17) is the equation of a tieline that connects a point defined by the composition of each stream entering the stage to a point that defines the equilibrium composition of the streams leaving the stage. The slope of this tieline is the ratio of the total equivalents of salt in the solution ($N_{To} v_o$) to the total equivalents of exchangeable ions in the zeolite ($W_o u_o$). The slope of the tielines usually remain constant in a multistage process. The isotherm for the K-Na-X system shown in Fig. 2 is repeated in Fig. 78. In this figure we illustrate how we calculate the number of theoretical stages required to produce a KNaX with 19.4% K in a crossflow process.

The feed conditions fix point (A) and the slope of the tieline, A-B. Extending the tieline to its intersection with the ion-exchange isotherm determines the other end of the tieline (B). The beginning point (C) for the tieline for the second stage is fixed by the solution fed to that stage and the equilibrium zeolite composition leaving the first stage. Again, the slope of the second tieline is determined from the stream entering the stage, and the end of the second tieline is fixed by where it intersects the ion exchange isotherm (D). This graphical process can be continued until the desired degree of ion exchange has been achieved. A material balance around the entire process will yield the total quantity of reactant required and the efficiency of utilization of the reactant. The number of theoretical stages, or contacts, is determined by counting the number of steps, or tielines, in the graph.

## D. Countercurrent Operation

The crossflow process is good for preparing laboratory samples but does not result in efficient use of the reactant (ion-exchange solution). Countercurrent ion exchange is a more desirable process. The flow diagram for the process is shown in Fig. 79. The working equation for countercurrent ion exchange is obtained by making material

Copyright © 2003 Marcel Dekker, Inc.

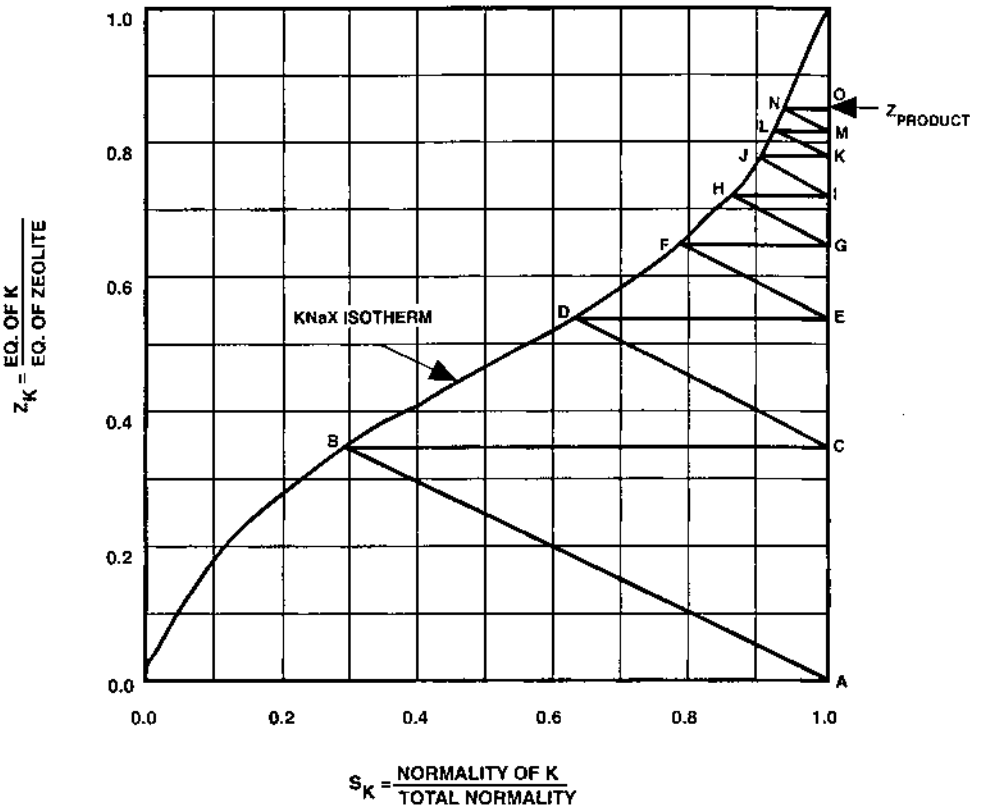


**Fig. 78** Calculation of the number theoretical stages required to produce KNaX containing 2.0% Na and 19.4% K in a crossflow process at 25° and 0.1 total normality (From Ref. 2.)

balance around the plant. Since the plant consist of $m$ stages we make a material balance around stage 1 through $m$ for the ingoing ion. The equation describing this material balance is

$$W_o u_o' Z_o + N_{Tm+1} V_{m+1}' S_{m+1} = W_m u_m' Z_m + N_{T1} v_1' S_1 \tag{18}$$

Solving for $Z_m$ with the aid of a pair of equations analogous to Eqs. (16a) and (16b) gives the following linear equation in $Z_m$ and $S_{m+1}$:

$$Z_m = C' S_{m+1}/Q' + Z_o - C' S_1/Q' \tag{19}$$

Equation (20) relates the concentration of the pairs of streams between any two stages in the countercurrent flow diagram. We can locate this line, the plant operating line, in an

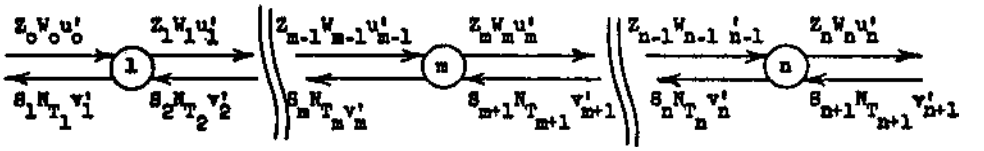


**Fig. 79** Flow diagram for countercurrent operation (From Ref. 2.)

Copyright © 2003 Marcel Dekker, Inc.

$S$, $Z$ coordinate system by allowing the $m$th stage to be the $n$th, or last stage in the process because

$$Z_n = Z_{\text{product}} \qquad S_{n+1} = S_{\text{feed}}$$
$$Z_o = Z_{\text{feed}} \qquad C'/Q' = \text{slope}$$

are specified and $S_1$, which is the concentration of the depleted exchange solution, can be obtained from Eq. (20) with the change in subscript.

Again using the K-Na-X isotherm from Fig. 2 in Fig. 80 we show the graphical calculation of the number of stages required to reach the desired degree of ion exchange, $Z_{\text{product}}$. The plant operation line is defined by fixing $Z_n$ ($= Z_{\text{product}}$), $S_{n+1}$ ($= S_{\text{feed}}$), and $C'/Q'$. It is simply drawn as shown in the figure.

The number of theoretical countercurrent stages required in this process is graphically computed. The point A defines the composition of the zeolite leaving the $n$th or last stage, $Z_{\text{product}}$, and the composition of the solution entering the last stage, $S_{\text{feed}}$. A horizontal line is drawn from point A to point B. The coordinates of point B are the equilibrium composition of the zeolite stream leaving the last stage, $Z_{\text{product}}$, and the solution, $S_n$, leaving the last stage and entering the $(n-1)$th stage. A vertical line is drawn from the point B to the intersection of the plant operating line, point C, which gives the composition of the zeolite entering the $n$th stage and leaving the $(n-1)$th stage. The points on this right angle "step," ABC , describe the concentrations of all of the streams entering

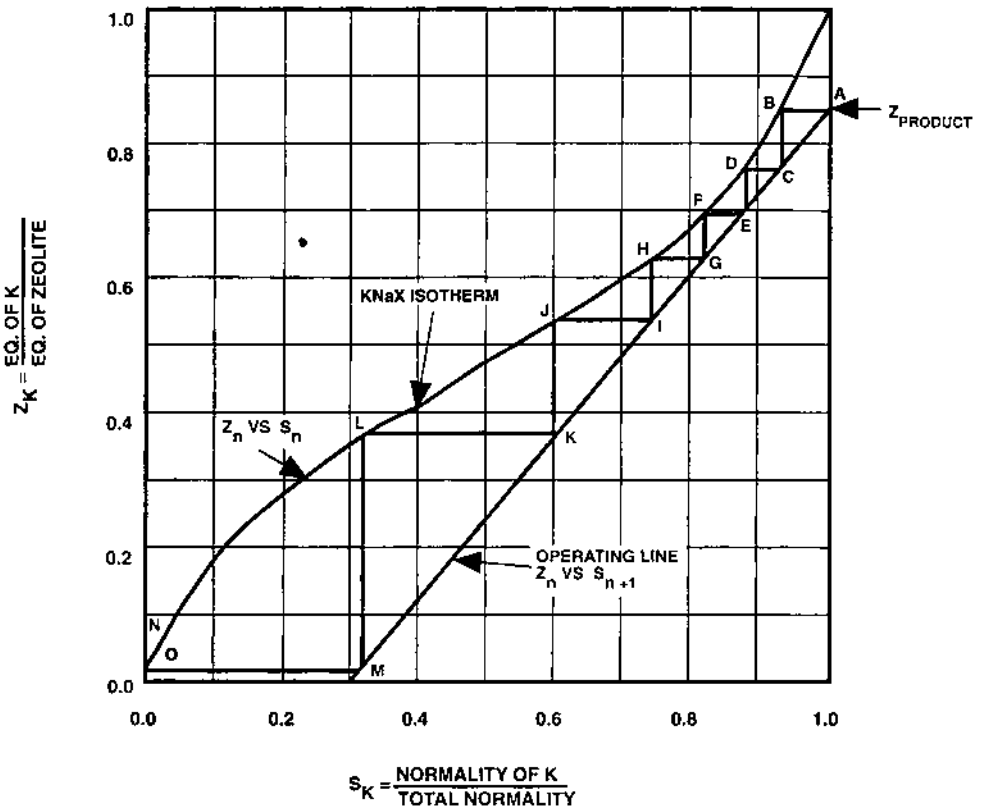


**Fig. 80** Example of the use of the graphical technique in countercurrent operation. (From Ref. 2.)

Copyright © 2003 Marcel Dekker, Inc.

and leaving the last stage. Realizing that the composition of the zeolite entering the $n$th stage and leaving the $(n-1)$th stage defines point D, a horizontal line is drawn from C to D. Since point D defines the composition of the zeolite stream and solution stream leaving the $(n-1)$th stage, a vertical line can be extended to the point E. This process of drawing a horizontal line from the plant operating line to the equilibrium isotherm and drawing a vertical line from the equilibrium isotherm to plant operating line can be continued until the point ($S = S$, $Z = Z_{\text{feed}}$) is reached. The number of theoretical stages needed to reach the zeolite composition, $Z_{\text{product}}$, starting from a composition, $Z_{\text{feed}}$, is simply the number of right angle "steps."

A theoretical stage is defined as one in which the zeolite and solution phases are in equilibrium and then a perfect phase separation is made. In a real process, equilibrium may not be reached and a perfect phase separation may not occur. A nonequilibrium isotherm may be used in this graphical process. Correction for imperfect separation of phases and salt imbibement is more difficult to do and becomes more important in very concentrated salt solutions.

## REFERENCES


1. L Gaines, HC Thomas. J Chem Phys 21:714–718, 1954.
2. HS Sherry. Zeolites 13:377–383,1993.
3. RM Barrer, JD Falconer. Proc R Soc (London) A236:227–249, 1956.
4. E Dempsey. Calculations on model crystals. Papers read at the Conference on Molecular Sieves, London, Soc. Chem. Ind., 1968, pp 203–305.
5. HS Sherry. J Phys Chem 70:1158–1168, 1966.
6. R Harjula, J Lehto, JH Pothius, A Dyer, RP Townsend. J Chem Soc 89:661, 1993.
7. HS Sherry. J Phys Chem 72:4086–4094, 1968.
8. RM Barrer, JA Davies, LVC Rees. J Inorg Nucl Chem 30:3333–3349, 1968.
9. RM Barrer, JA Davies, LVC Rees. J Inorg Nucl Chem 31:2599–2609, 1969.
10. RM Barrer, LVC Rees, J Shamsuzzoha. J Inorg Nucl Chem 28:629–642, 1966.
11. WM Meier, DH Olson. Zeolites 12:122–123, 1992.
12. WH Bauer. Am Mineral 49:697, 1964.
13. L Broussard, DP Shoemaker. J Am Chem Soc 82:1041, 1960.
14. DH Olson. J Phys Chem 74:2758, 1970.
15. L Pauling. The Nature of the Chemical Bond. Ithaca, NY: Cornell University Press, 1960, p 514.
16. D Rosseinsky. Chem Rev 65:467, 1965.
17. DH Olson, HS Sherry. J Phys Chem 72:4095–4104, 1968.
18. RM Barrer, L Hinds. J Chem Soc 1870–1888, 1953.
19. BK Theng, E Vansant, JB Uytterhoeven. Trans Faraday Soc 64:3370–3382, 1968.
20. HS Sherry. J Colloid Interf Sci 28:288–293, 1968.
21. HS Sherry, AB Schwartz. US Patent No. 3,677,698 (July 18, 1972).
22. HS Sherry. J Colloid Interf Sci 36:321–331, 1976.
23. DH Olson, Gt Kokotailo, JF Charnell. J Colloid Interf Sci 28, 1968.
24. JG Nery, YP Mascarencas, TJ Bonagamba, NC Mello. Zeolites 18:44–49, 1997.
25. RM Barrer, JD Falconer. Proc R Soc (London) A236:227–249, 1956.
26. RM Barrer, WM Meier. Trans Faraday Soc 54:1074–1085, 1958.
27. HS Sherry, HF Walton. J Phys Chem 71:1457–1465, 1967.
28. EP Hertzenberg, HS Sherry. In: WH Flank, ed. ACS Symposium Series 135. Washington, DC: American Chemical Society, 1980, pp 187–198.
29. JF O'Connor, RP Townsend. Zeolites 5:158–164, 1985.
30. HS Sherry. Ion Exchange Properties of the Synthetic Zeolite, Linde T. Papers read at the Meeting on Ion Exchange in the Process Industries London: Soc. Chem. Ind.1970, pp 329–337.


Copyright © 2003 Marcel Dekker, Inc.

31. JM Bennett, JA Gard. Nature 214:1005, 1967.
32. HS Sherry. Clays Clay Minerals 27:231–237, 1979.
33. A Dyer, M Zubair. Micropor Mesopor Mater 22:135–150, 1998.
34. A Langella, M Pansini, P Cappelletti, B de Gennaro, M de Gennaro, C Collella. Micropor Mesopor Mater 37:337–343, 2000.
35. RM Barrer, H Villiger. Z Kristallogr 128:352, 1969.
36. PA Newell, LVC Rees. Zeolites 3:22–27, 1983.
37. P Fletcher, RP Townsend. Zeolites 3:129–133, 1983.
38. P Fletcher, RP Townsend. J Chem Soc Faraday Trans I, 78:1741, 1982.
39. P Chu, FG Dwyer. Zeolites 3:72–76, 1983.
40. R Rinaldi, JJ Pluth, JV Smith. Acta Crystallogr 31 Section B:1603, 1975.
41. P Chu, FG Dwyer. In: G Stuckey, ed. Intrazeolite Chemistry. Washington, DC: Am Chem Soc, 1988, pp 59–78.
42. DP Matthews, LVC Rees. In: TSR Prasado Rao, ed. Advances in Catalysis Science and Technology. New Dehli: Wiley Eastern Ltd, 1985, p 493.
43. AM McAleer, LVC Rees, AK Nowak. Zeolites 11:329–336, 1991.
44. HS Sherry. In: JA Marinsky, ed. Advances in Ion Exchange, Vol 2. New York: Marcel Dekker, 1969, pp 89–133.
45. P Chu, FG Dwyer. Zeolites 8:423–426, 1988.
46. GT Kokotailo et al. Nature 275:119, 1978.
47. TC Watling, LVC Rees. Zeolites 14:687–692, 1994.
48. TC Watling, LVC Rees. Zeolites 14:693–696, 1994.
49. F Hellferich. Ion Exchange. New York: McGraw-Hill, 1962, pp 134–140.
50. W Platek, JA Marinsky. J Phys Chem 65:2118–2122, 1961.
51. RM Barrer, W Meier. J Chem Soc 1958:199.
52. RM Barrer, AJ Walker. Trans Faraday Soc 60:171, 1964.

Copyright © 2003 Marcel Dekker, Inc.